

5 Cluster Extensions of Dynamical Mean-Field Theory

Michael Potthoff

Department of Physics, University of Hamburg
Jungiusstraße 9, D-20355 Hamburg

Contents

1	Introduction	2
2	Lattices, reciprocal lattices, and superlattices	5
3	Discrete Fourier transformations	7
4	Single-electron Green function	9
5	Local and nonlocal correlations	11
6	Cluster perturbation theory	14
7	Periodization schemes	16
8	Self-consistent cluster-embedding approaches	21
9	Discussion of selected results	26
10	Conclusions and open problems	30

1 Introduction

Cluster extensions of dynamical mean-field theory (DMFT) are popular approximation schemes developed for systems of interacting electrons on low-dimensional lattices with local interactions to get access to their thermal equilibrium properties and to their single-electron excitations. This topic came up soon after the development of dynamical mean-field theory [1–4] and has been reviewed in a couple of papers [4–6]. Important milestones defining the field begin with the proposal for a *dynamical cluster approximation* (DCA) in 1998 [7], a cluster extension formulated in reciprocal \mathbf{k} -space. The real-space perspective was emphasized in 2000 [8] with a cluster DMFT approach applied to the two-dimensional Hubbard model. Its formal framework is the *cellular dynamical mean-field theory* (C-DMFT), suggested in 2001 [9]. An alternative simplified cluster approach, the *variational cluster approach* (VCA) was introduced in 2003 [10]. All cluster approaches rely on a number of basic concepts, such as the many-body problem, lattice-fermion models, the mean-field idea, and the DMFT itself.

The many-body problem is a complexity problem. For a classical or quantum system consisting of a few particles the fundamental equations of motion can be solved analytically or at least numerically with machine precision. Condensed-matter theory, however, is confronted with many-particle systems, in particular with quantum systems with a macroscopic number of electrons. In these cases, to aim at the complete information on the microscopic degrees of freedom is a meaningless concept, and a quantum-statistical approach must be employed. Most of the experimentally accessible macroscopic system properties are described by thermodynamics in a phenomenological way and are derived from the underlying laws of microscopic fundamental interactions by statistical physics. The thermodynamics of a macroscopically large system of valence electrons is completely determined by a thermodynamical potential $F(T, \mu, x)$, which depends on temperature T , the chemical potential μ , and other macroscopic control parameters x . Its direct computation via $F = -T \ln Z(T, \mu, x)$ from the grand partition function $Z(T, \mu, x) = \text{Tr} \exp(-\beta(H(x) - \mu N))$ (with $\beta = 1/T$, $k_B \equiv 1$) is practically impossible for generic Hamiltonians $H(x)$ since the trace is actually a high-dimensional sum over a Fock-space basis. Hence, approximations are inevitable.

DMFT and its cluster extensions aim at a description of *strongly interacting electron systems*. The presence of interactions prohibits a simple factorization of the partition function, $Z = \prod_k Z_k$, into simple partition functions Z_k for the different one-particle degrees of freedom, which is known from the textbook treatment of the noninteracting Fermi gas. The Coulomb interaction, which is the relevant type of interaction for almost all interesting properties of condensed matter, must be regarded as “strong”, meaning that a perturbative theoretical approach is expected to fail. On the other hand, strongly interacting electron systems are highly interesting. Interactions are responsible for many famous collective quantum effects which only show up in interacting quantum Fermi systems in the thermodynamic limit. Some examples are the Kondo effect, i.e., the collective screening of a magnetic moment by a mesoscopically large number of valence electrons in states close to the Fermi energy [11], collective magnetism, i.e., the collective order of magnetic moments below a characteristic transition temperature [12, 13],

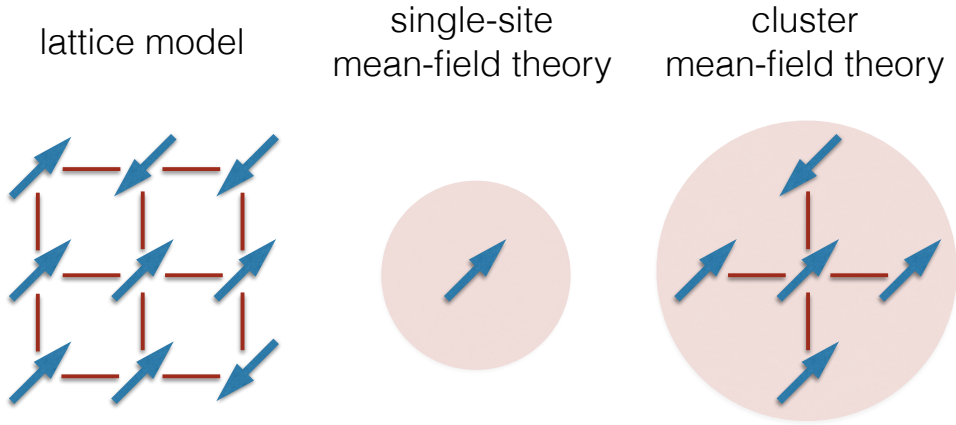


Fig. 1: Left: Spin configuration of the Ising model on the square lattice. Middle: Ising spin in a mean field. Right: Configuration of an Ising-spin cluster in a mean field.

unconventional high-temperature superconductivity [14, 15], or interaction-induced Mott insulating behavior [16]. The essence of those effects is captured with surprisingly simple lattice fermion or effective spin models, such as the Hubbard and the Heisenberg model, the Kondo-lattice model, the periodic Anderson model, other multi-orbital lattice models etc.

The *mean-field approach* to strongly interacting lattice fermion models is borrowed from the simple Weiss theory of the Ising model, see Fig. 1. For the Ising model with nearest-neighbor exchange J between spin $S_i = \pm 1$ on the $D = 2$ -dimensional square lattice with L sites, the left panel shows one of the 2^L spin configurations which must be summed over in an exact computation of the partition function. Note that the number of configurations increases exponentially with L . The middle panel sketches the idea of a single-site mean-field theory. It takes a local point of view and picks a representative spin S_i at site i which experiences a fluctuating local field $\sim J \sum_{j=1}^{2D} S_j$ created by the spin exchange with its $2D$ nearest neighbors. In the mean-field approximation, this fluctuating local field is replaced by a constant mean field B_{eff} . Note that, due to the central-limit theorem, this replacement can be justified in the limit of infinite dimensions $D \rightarrow \infty$. The mean or Weiss field adds to a possibly nonzero physical magnetic field B . Correspondingly, the exact Ising Hamiltonian is replaced by a mean-field Hamiltonian $H_{\text{MF}} = -(B_{\text{eff}} + B) \sum_i S_i$. This implies a dramatic simplification of the original model as the partition function factorizes. One must merely solve the remaining impurity problem, i.e., a *single* spin coupled to a mean field or ‘‘bath’’. As the bath actually represents the average nearest-neighbor spin configuration, it should be calculated from the thermal expectation value of S_i . Hence, the solution of the impurity problem and the determination of the bath must be done self-consistently, and the condition fixing the bath is therefore called the *self-consistency condition*. A mean-field theory replaces a lattice model by an impurity model where the impurity is self-consistently embedded in a bath.

Dynamical mean-field theory is in many respects the optimal mean-field theory for a lattice-fermion model like the Hubbard model as a prototype. It self-consistently maps the original

model onto a much simpler reference system which consists of a fermionic impurity, a Hubbard site, for example, which is embedded in a continuum of fermionic bath degrees of freedom. It is not surprising that this bath is much more complicated compared to the bath in the Weiss theory of the simple classical Ising model and that fixing the continuous bath requires a quite different self-consistency condition opposed to fixing a single number, namely B_{eff} , in the case of the Ising system. The formulation in fact requires a frequency-dependent one-particle Green function and thus explains the term *dynamical* mean-field theory as opposed to the static Weiss theory. The DMFT is a big landmark in the landscape of various mean-field-like approximation techniques and serves as a point of orientation, as it combines a number of attractive features: The theory is formally not restricted to certain parameter ranges, such as weak interaction, low density etc. It works without internal inconsistencies in the entire parameter regime of the model under consideration. In this sense, it is a nonperturbative theory. The DMFT can be seen as the exact theory of the lattice-fermion model in a special limit, namely for an infinite-dimensional lattice. This limit, however, must be defined carefully to keep the balance between the one- and the two-body terms in the Hamiltonian. The power of DMFT very much results from the fact that the according $D = \infty$ models are highly nontrivial with nontrivial phase diagrams, excitation spectra, and also nontrivial real-time dynamics. Usually, however, it is employed as an approximation to treat finite-dimensional lattice models. The DMFT is able to describe spontaneous symmetry breaking and states of matter with collective order, such as magnetism, superconductivity, charge order, orbital order etc. It is a beautiful and robust theory on the formal level, which can be derived in various ways and starting from various setups. Most importantly, however, DMFT has turned out as highly successful in practice, including particularly applications to real materials which so far, on the conventional basis of density-functional theory and the local-density approximation, could not be addressed properly since strong electron correlations are essential for their observable properties.

Still, there are a couple of remaining problems which are related to the mean-field character and the local nature of the theory. For example, while DMFT is able to describe phases with long-range order, it insufficiently treats short-range correlations, particularly the feedback of short-range magnetic correlations on the one-electron Green function. It can describe two-particle correlation functions, such as the spin-structure factor or the conductivity but those do not affect the self-consistent determination of the bath. This has decisive consequences for the application to low-dimensional lattice models and can result in qualitatively wrong phase diagrams. In fact, as will be discussed later, it can spectacularly fail for models in $D = 2$ dimensions. Furthermore, the restriction to a single-site impurity implies that the DMFT cannot describe symmetry-broken phases with nonlocal order parameters, which unfortunately includes unconventional d -wave superconductivity. DMFT also shares with all mean-field-like theories the inability to predict the correct critical behavior in the parametric vicinity of second-order phase transitions, it violates exact Ward identities and theorems such as the Mermin-Wagner theorem [17]. Clearly, DMFT cannot be the end of the story as it is approximative when applied to a finite-dimensional lattice model. What is needed here is a systematic route starting from DMFT towards the exact solution.

One idea, and this is the theme of this review and lecture, is to extend the self-consistent embedding of a single site to an embedding of a cluster consisting of several sites L_c . This is displayed in the right panel of Fig. 1. Without having detailed the precise form of a cluster extension of the DMFT, it is already clear that this is a systematic approach to the full solution. There is simply no need for a self-consistent embedding of a cluster cut out of an infinite lattice-fermion model if the cluster itself has infinite size. On the other hand, it is also obvious from the beginning that the computational effort will drastically increase with increasing L_c . The construction of a cluster DMFT should therefore be guided by the goal to achieve fast convergence for $L_c \rightarrow \infty$. We will see that there is more than one way to perform this construction, and we will also see some common intrinsic advantages and deficiencies of the cluster approach as such.

2 Lattices, reciprocal lattices, and superlattices

To develop the formal framework of cluster extensions of DMFT, we will first discuss some geometrical issues. We start with a D -dimensional Bravais lattice spanned by the basis vectors $\mathbf{a}_1, \dots, \mathbf{a}_D$. The points of the lattice are given by lattice vectors

$$\mathbf{R} \equiv \mathbf{R}_i = \sum_{\alpha=1}^D i_{\alpha} \mathbf{a}_{\alpha}, \quad (1)$$

where $i = (i_1, \dots, i_D)$ with arbitrary integers $i_{\alpha} \in \mathbb{Z}$. For each lattice, we have a reciprocal lattice which is spanned by the basis vectors $\mathbf{b}_1, \dots, \mathbf{b}_D$. These are defined as the unique solution of the linear system of equations

$$\mathbf{a}_{\alpha} \mathbf{b}_{\beta} = 2\pi \delta_{\alpha\beta}. \quad (2)$$

Points in the reciprocal lattice are given by reciprocal lattice vectors

$$\mathbf{G} \equiv \mathbf{G}_j = \sum_{\beta=1}^D j_{\beta} \mathbf{b}_{\beta}, \quad (3)$$

where $j = (j_1, \dots, j_D)$ with $j_{\beta} \in \mathbb{Z}$. The parallelepiped defined by the basis $\mathbf{a}_1, \dots, \mathbf{a}_D$ is a primitive cell \mathcal{C} of the lattice, whereas $\mathbf{b}_1, \dots, \mathbf{b}_D$ define a primitive cell of the reciprocal lattice, a reciprocal unit cell \mathcal{RC} . For their volumes we have the relation $V_{\mathcal{C}} V_{\mathcal{RC}} = (2\pi)^D$. Primitive cells are not unique. Another reciprocal unit cell, with higher symmetry group, is the well-known Brillouin zone (\mathcal{BZ}).

There is a symmetry between the original and reciprocal lattice. We immediately have the identity

$$\exp(i\mathbf{G}\mathbf{R}) = 1, \quad (4)$$

and the reciprocal lattice of the reciprocal lattice is the original lattice. The reciprocal lattice can be used to expand a function $f(\mathbf{x})$ that is lattice periodic, $f(\mathbf{x} + \mathbf{R}_i) = f(\mathbf{x})$, in a Fourier series

$$f(\mathbf{x}) = \sum_{\mathbf{G}} f_{\mathbf{G}} e^{i\mathbf{G}\mathbf{x}}, \quad f_{\mathbf{G}} = \frac{1}{V_{\mathcal{C}}} \int_{\mathcal{C}} d^D r f(\mathbf{x}) e^{-i\mathbf{G}\mathbf{x}}. \quad (5)$$

object, quantity	symbol, definition	properties, relations
basis spanning the lattice volume of a primitive cell lattice vectors	\mathbf{a}_α $V_C = \det(\{\mathbf{a}_\alpha\})$ $\mathbf{R} = \mathbf{R}_i = \sum_\alpha i_\alpha \mathbf{a}_\alpha$	$\alpha = 1, \dots, D$ $i_\alpha \in \mathbb{Z}, 1 \leq i_\alpha \leq L_\alpha$
basis vectors of reciprocal lattice volume of a reciprocal unit cell reciprocal lattice vectors	\mathbf{b}_β $V_{RC} = \det(\{\mathbf{b}_j\})$ $\mathbf{G} = \mathbf{G}_j = \sum_\beta j_\beta \mathbf{b}_\beta$	$\mathbf{a}_\alpha \mathbf{b}_\beta = 2\pi \delta_{\alpha\beta}$ $V_{RC} = (2\pi)^D / V_C$ $j_\beta \in \mathbb{Z}, \mathbf{G}\mathbf{R} \in 2\pi\mathbb{Z}$
basis spanning the superlattice volume of a superlattice cell superlattice vectors	$\tilde{\mathbf{a}}_\alpha$ $V_{SC} = \det(\{\tilde{\mathbf{a}}_\alpha\})$ $\tilde{\mathbf{R}} = \tilde{\mathbf{R}}_i = \sum_\alpha i_\alpha \tilde{\mathbf{a}}_\alpha$	$\tilde{\mathbf{a}}_\alpha = L_{c,\alpha} \mathbf{a}_\alpha$ $V_{SC} = L_c V_C$ $i_\alpha \in \mathbb{Z}, 1 \leq i_\alpha \leq L / L_{c,\alpha}$
basis of reciprocal superlattice volume of a rec. superlattice cell reciprocal superlattice vectors	$\tilde{\mathbf{b}}_\beta$ $V_{RSC} = \det(\{\tilde{\mathbf{b}}_j\})$ $\tilde{\mathbf{G}} = \tilde{\mathbf{G}}_j = \sum_\beta j_\beta \tilde{\mathbf{b}}_\beta$	$\tilde{\mathbf{a}}_\alpha \tilde{\mathbf{b}}_\beta = 2\pi \delta_{\alpha\beta}$ $V_{RSC} = (2\pi)^D / V_{SC}$ $\tilde{\mathbf{G}}\tilde{\mathbf{R}} \in 2\pi\mathbb{Z}$
vectors spanning the system system volume	\mathbf{A}_α $V = \det(\{\mathbf{A}_i\})$	$\mathbf{A}_\alpha = L_\alpha \mathbf{a}_\alpha = (L / L_{c,\alpha}) \tilde{\mathbf{a}}_\alpha$ $V = L V_C$
discrete wave vectors volume element in \mathbf{k} -space	\mathbf{k} $\Delta^D k$	$\mathbf{k}\mathbf{A}_\alpha \in 2\pi\mathbb{Z}$ $\Delta^D k = (2\pi)^D / V$

Table 1: Overview of the various quantities defining the lattice and the reciprocal lattice, the system volume and the \mathbf{k} -space.

On a suitably defined Hilbert space of functions $f(\mathbf{x})$, this expansion results from the fact that the functions $\exp(i\mathbf{G}\mathbf{x})$ form an orthonormal basis: $\frac{1}{V_C} \int_C d^D r e^{-i\mathbf{G}\mathbf{x}} e^{i\mathbf{G}'\mathbf{x}} = \delta_{\mathbf{G},\mathbf{G}'}$. A completely analogous construction can be made for functions $g(\mathbf{p})$ with $g(\mathbf{p} + \mathbf{G}_j) = g(\mathbf{p})$. While one is eventually interested in the properties of a lattice-fermion model, such as the Hubbard model, on a lattice with an infinite number of lattice sites L , it is convenient to first consider a *finite* lattice and to solve the problem for $L < \infty$,

$$L = L_1 \times \cdots \times L_D, \quad (6)$$

and a certain finite number of fermions N , and finally to perform the thermodynamical limit $L \rightarrow \infty$, $N \rightarrow \infty$ with $n \equiv N/L = \text{const}$. This raises the question of boundary conditions. Excluding systems in a critical state, where system properties are infinitely susceptible to small perturbations, the precise form of the boundary conditions does not matter in the thermodynamic limit. In the case of open boundaries, the system volume is spanned by a set of vectors $\mathbf{A}_1, \dots, \mathbf{A}_D$, such that the system volume is $V = \det(\mathbf{A}_1, \dots, \mathbf{A}_D)$. We should impose consistency constraints, $\mathbf{A}_\alpha = L_\alpha \mathbf{a}_\alpha$, to respect the underlying lattice structure.

Periodic boundary conditions are much more convenient. Here, we identify vectors \mathbf{x} and $\mathbf{x} + \mathbf{A}_i$. The geometrical perspective is that the macroscopic system topology is that of a D -dimensional torus T^D . An equivalent point of view is that all real-space functions $f(\mathbf{x})$ with $\mathbf{x} \in \mathbb{R}^D$ respect the conditions $f(\mathbf{x} + \mathbf{A}_i) = f(\mathbf{x})$ and, therefore, can be expanded in a Fourier series, $f(\mathbf{x}) = \sum_{\mathbf{k}} \exp(i\mathbf{k}\mathbf{x}) f_{\mathbf{k}}$, where the wave vectors \mathbf{k} can be seen as the reciprocal-lattice vectors of the real-space lattice spanned by $\mathbf{A}_1, \dots, \mathbf{A}_D$. Hence, $\exp(i\mathbf{k}\mathbf{A}_i) = 1$, and the volume

element in \mathbf{k} space is $\Delta^D k = (2\pi)^D/V$. This also implies that the number of \mathbf{k} -points in the reciprocal unit cell, $V_{\mathcal{RC}}/\Delta^D k$, equals the number of sites in the system L , since

$$\Delta^D k = \frac{(2\pi)^D}{V} = \frac{(2\pi)^D}{V_c} \frac{V_c}{V} = V_{\mathcal{RC}} \frac{1}{L}. \quad (7)$$

Some overview of the notations used and of the basic relations is given in table 1.

For cluster extensions of the DMFT, there is a third pair of lattice and corresponding reciprocal lattice to be considered. The original lattice of L sites is tiled into L/L_c identical clusters with a finite number of L_c sites each. Each of the identical clusters has a cluster origin, which can be chosen as a particular site in the cluster, such that all cluster origins are equivalent and form a *superlattice*. We define the primitive vectors of the superlattice $\tilde{\mathbf{a}}_\alpha$ for $\alpha = 1, \dots, D$, and we impose consistency constraints, such as $\tilde{\mathbf{a}}_\alpha = L_{c,\alpha} \mathbf{a}_\alpha$ in the most simple case, to respect the underlying lattice structure. Hence, the number of cluster sites is given by $L_c = L_{c,1} \times \dots \times L_{c,D}$. The volume of the unit cell of the superlattice is given by $V_{Sc} = \det(\{\tilde{\mathbf{a}}_\alpha\})$, and we have $V_{Sc} = L_c V_c = (L_c/L)V$.

The reciprocal superlattice consists of the vectors $\tilde{\mathbf{G}} \equiv \tilde{\mathbf{G}}_j = \sum_\beta j_\beta \tilde{\mathbf{b}}_\beta$ and is spanned by the basis of the reciprocal superlattice $\{\tilde{\mathbf{b}}_\beta\}$ with $j = (j_1, \dots, j_D) \in \mathbb{Z}^D$. The real-space consistency constraints imply that $\tilde{\mathbf{b}}_\beta = \mathbf{b}_\beta / L_{c,\beta}$. We have $\exp(i\tilde{\mathbf{G}} \tilde{\mathbf{R}}) = 1$, where $\tilde{\mathbf{R}} \equiv \tilde{\mathbf{R}}_i = \sum_\alpha i_\alpha \tilde{\mathbf{a}}_\alpha$ are the superlattice vectors. Furthermore, the number of reciprocal superlattice vectors in the reciprocal unit cell, $V_{\mathcal{RC}}/V_{Sc}$, is given by L_c , since

$$V_{Sc} = \frac{(2\pi)^D}{V_{Sc}} = \frac{(2\pi)^D}{V_c} \frac{V_c}{V_{Sc}} = V_{\mathcal{RC}}/L_c. \quad (8)$$

Fig. 2 provides an example of a $D = 2$ -dimensional lattice.

3 Discrete Fourier transformations

Figure 2 also demonstrates that any lattice vector

$$\mathbf{R} = \tilde{\mathbf{R}} + \mathbf{r} \quad (9)$$

can be uniquely decomposed into a vector of the superlattice $\tilde{\mathbf{R}}$, i.e., the position vector to the respective cluster origin, and a position vector \mathbf{r} to the respective site in the cluster, referring to the cluster origin. Note that there are L lattice points \mathbf{R} , and L/L_c clusters with L_c sites each. Vice versa, for a given wave vector \mathbf{k} there is the unique decomposition

$$\mathbf{k} = \tilde{\mathbf{k}} + \tilde{\mathbf{G}}, \quad (10)$$

where $\tilde{\mathbf{G}}$ are the reciprocal superlattice vectors. Note that in a reciprocal unit cell there are L wave vectors \mathbf{k} and L_c reciprocal superlattice vectors $\tilde{\mathbf{G}}$, and there are L/L_c wave vectors $\tilde{\mathbf{k}}$.

Let us consider the $L \times L$ matrix \mathbf{U} with elements

$$U_{\mathbf{R},\mathbf{k}} = \frac{1}{\sqrt{L}} e^{i\mathbf{k}\mathbf{R}}, \quad \mathbf{k} \in \mathcal{RC}, \quad (11)$$

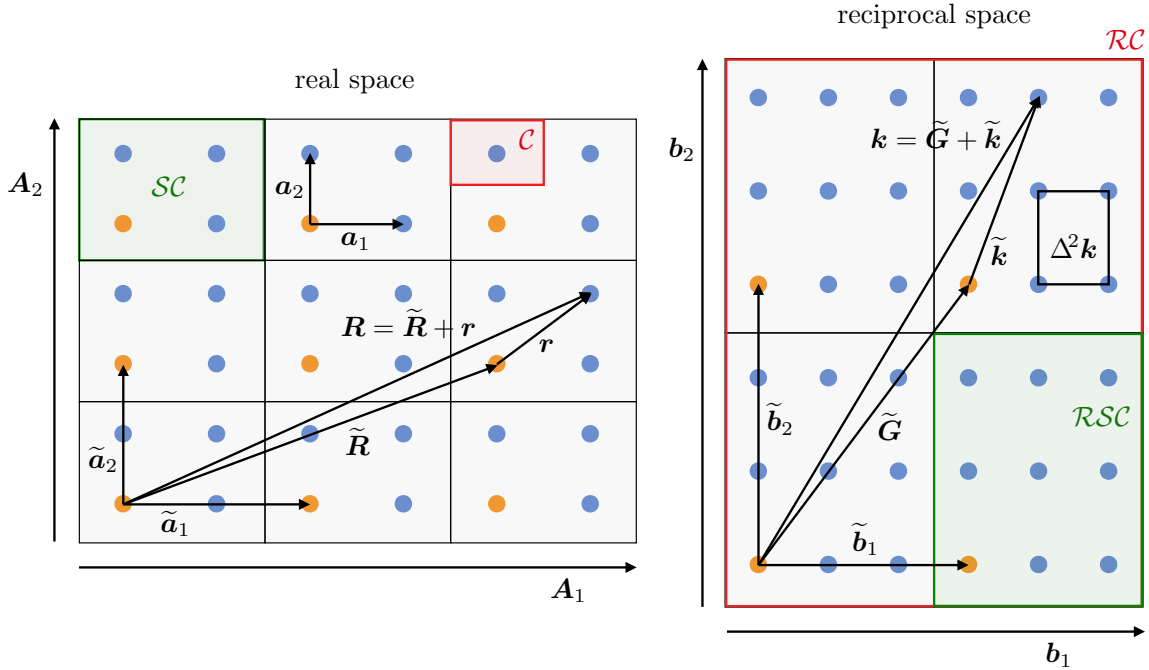


Fig. 2: Example of a lattice/superlattice in $D = 2$ dimensions. Real space, left: A system consisting of $L = 36$ sites on a square lattice with periodic boundary conditions. \mathcal{C} : unit cell. $\mathbf{a}_1, \mathbf{a}_2$: basis vectors of the lattice. Lines: tiling into clusters with $L_c = 4$ sites. Orange sites: cluster origins, forming a superlattice structure of $L/L_c = 9$ clusters. \mathcal{SC} : unit cell of the superlattice. $\tilde{\mathbf{a}}_1, \tilde{\mathbf{a}}_2$: superlattice basis vectors. Any lattice vector \mathbf{R} can be decomposed uniquely into a superlattice vector $\tilde{\mathbf{R}}$ and a cluster vector \mathbf{r} . $\mathbf{A}_1, \mathbf{A}_2$: primitive translations defining the periodic boundary conditions and the total system size. Reciprocal space, right: $\mathbf{b}_1, \mathbf{b}_2$ reciprocal basis spanning a reciprocal unit cell \mathcal{RC} containing $L = 36$ \mathbf{k} -points. $\Delta^2 \mathbf{k} = (2\pi)/V$: volume element. The \mathcal{RC} contains $L_c = 4$ reciprocal supercells (\mathcal{RSC}) with $L/L_c = 9$ wave vectors $\tilde{\mathbf{k}}$ each. Their volume is $V_{\mathcal{RSC}} = V_{\mathcal{RC}}/L_c$. Any wave vector \mathbf{k} can be decomposed uniquely into a reciprocal superlattice vector $\tilde{\mathbf{G}}$ and a wave vector $\tilde{\mathbf{k}}$.

and the $L/L_c \times L/L_c$ matrix \mathbf{V} with elements

$$V_{\tilde{\mathbf{R}}, \tilde{\mathbf{k}}} = \frac{1}{\sqrt{L/L_c}} e^{i\tilde{\mathbf{k}}\tilde{\mathbf{R}}}, \quad \tilde{\mathbf{k}} \in \mathcal{RSC}, \quad (12)$$

and the $L_c \times L_c$ matrix \mathbf{W} with elements

$$W_{\mathbf{r}, \tilde{\mathbf{G}}} = \frac{1}{\sqrt{L_c}} e^{i\tilde{\mathbf{G}}\mathbf{r}}, \quad \tilde{\mathbf{G}} \in \mathcal{RC}. \quad (13)$$

The unitary matrices \mathbf{U} , \mathbf{V} and \mathbf{W} define discrete Fourier transformations between the respective real and reciprocal spaces. We refer to the different transformations as the lattice Fourier transformation (\mathbf{U}), the superlattice Fourier transformation (\mathbf{V}), and the cluster Fourier transformation (\mathbf{W}). For example, one can straightforwardly prove that

$$\frac{1}{L} \sum_{\mathbf{R}} e^{-i(\mathbf{k}-\mathbf{k}')\mathbf{R}} = \sum_{\mathbf{R}} U_{\mathbf{k}, \mathbf{R}}^\dagger U_{\mathbf{R}, \mathbf{k}'} = \delta_{\mathbf{k}, \mathbf{k}'}, \quad \frac{1}{L} \sum_{\mathbf{k}} e^{i\mathbf{k}(\mathbf{R}-\mathbf{R}')} = \sum_{\mathbf{k}} U_{\mathbf{R}, \mathbf{k}} U_{\mathbf{k}, \mathbf{R}'}^\dagger = \delta_{\mathbf{R}, \mathbf{R}'} \quad (14)$$

and thus, for some \mathbf{R} -dependent observable $O_{\mathbf{R}}$,

$$O_{\mathbf{k}} = \frac{1}{\sqrt{L}} \sum_{\mathbf{R}} e^{i\mathbf{k}\mathbf{R}} O_{\mathbf{R}}, \quad O_{\mathbf{R}} = \frac{1}{\sqrt{L}} \sum_{\mathbf{k}} e^{-i\mathbf{k}\mathbf{R}} O_{\mathbf{k}}. \quad (15)$$

Analogous relations hold for the other two cases. The formal structure of the proof is the same in all cases. Although there is a one-to-one relation between \mathbf{R} and $(\tilde{\mathbf{R}}, \mathbf{r})$ and between \mathbf{k} and $(\tilde{\mathbf{k}}, \tilde{\mathbf{G}})$, the lattice Fourier transformation \mathbf{U} involving lattice vectors \mathbf{R} cannot be decomposed into the superlattice transformation involving superlattice vectors $\tilde{\mathbf{R}}$ and the cluster transformation involving cluster vectors \mathbf{r} , i.e., $\mathbf{U} \neq \mathbf{VW} = \mathbf{WV}$. We note that a quantity $A_{\mathbf{R}, \mathbf{R}'}$ which is invariant under lattice translations \mathbf{R}_0 , i.e. $A_{\mathbf{R} + \mathbf{R}_0, \mathbf{R}' + \mathbf{R}_0} = A_{\mathbf{R}, \mathbf{R}'}$, is diagonalized by \mathbf{U} : $(\mathbf{U}^\dagger \mathbf{A} \mathbf{U})_{\mathbf{k}\mathbf{k}'} = A(\mathbf{k}) \delta_{\mathbf{k}, \mathbf{k}'}$. A quantity $A_{\mathbf{R}, \mathbf{R}'}$ which is invariant under superlattice translations $\tilde{\mathbf{R}}_0$ as well as under cluster translations \mathbf{r}_0 (i.e., which is cyclic on the cluster), $A_{\mathbf{R} + \tilde{\mathbf{R}}_0, \mathbf{R}' + \tilde{\mathbf{R}}_0} = A_{\mathbf{R} + \mathbf{r}_0, \mathbf{R}' + \mathbf{r}_0} = A_{\mathbf{R}, \mathbf{R}'}$, is diagonalized by \mathbf{VW} : $(\mathbf{W}^\dagger \mathbf{V}^\dagger \mathbf{A} \mathbf{VW})_{\tilde{\mathbf{k}}\tilde{\mathbf{G}}, \tilde{\mathbf{k}}'\tilde{\mathbf{G}}'} = A(\tilde{\mathbf{k}}, \tilde{\mathbf{G}}) \delta_{\tilde{\mathbf{k}}, \tilde{\mathbf{k}'}} \delta_{\tilde{\mathbf{G}}, \tilde{\mathbf{G}'}}$.

4 Single-electron Green function

DMFT and its cluster extensions are theories based on the single-particle Green function $G_{\mathbf{R}, \mathbf{R}'}(\omega)$ which, at $T = 0$, for complex $\omega \neq \mathbb{R}$ (and using units with $\hbar = 1$) is defined as

$$G_{\mathbf{R}, \mathbf{R}'}(\omega) = \left\langle 0 \left| c_{\mathbf{R}', \sigma}^\dagger \frac{1}{\omega - E_0 + H} c_{\mathbf{R}, \sigma} \right| 0 \right\rangle + \left\langle 0 \left| c_{\mathbf{R}, \sigma} \frac{1}{\omega + E_0 - H} c_{\mathbf{R}', \sigma}^\dagger \right| 0 \right\rangle. \quad (16)$$

Here, $c_{\mathbf{R}, \sigma}^\dagger$ is the creation operator of an electron with spin projection $\sigma = \uparrow, \downarrow$ at lattice site \mathbf{R} , and $c_{\mathbf{R}, \sigma}$ is the corresponding annihilator. $|0\rangle$ is the ground state of the Hamiltonian H , and E_0 is the ground-state energy. Note that $1/(\dots)$ stands for the operator inverse. We assume that H is spin-independent, such that the Green function is diagonal in the spin-projection indices and spin-independent. Furthermore, H shall be invariant under lattice translations, $c_{\mathbf{R}, \sigma} \rightarrow c_{\mathbf{R} + \mathbf{R}_0, \sigma}$ and $c_{\mathbf{R}, \sigma}^\dagger \rightarrow c_{\mathbf{R} + \mathbf{R}_0, \sigma}^\dagger$. Then, the Green function is invariant under lattice translations as well,

$$G_{\mathbf{R} + \mathbf{R}_0, \mathbf{R}' + \mathbf{R}_0}(\omega) = G_{\mathbf{R}, \mathbf{R}'}(\omega). \quad (17)$$

This implies that the matrix $\mathbf{G}(\omega)$ with elements $G_{\mathbf{R}, \mathbf{R}'}(\omega)$ is diagonalized by the lattice Fourier transformation

$$(\mathbf{U}^\dagger \mathbf{G}(\omega) \mathbf{U})_{\mathbf{k}\mathbf{k}'} = G(\mathbf{k}, \omega) \delta_{\mathbf{k}, \mathbf{k}'}. \quad (18)$$

From the retarded Green function $\mathbf{G}^{(\text{ret})}(\omega) \equiv \lim_{\eta \searrow 0} \mathbf{G}(\omega + i\eta) \equiv \mathbf{G}(\omega + i0^+)$ with $\omega \in \mathbb{R}$ we obtain the spectral density

$$A(\mathbf{k}, \omega) = -\frac{1}{\pi} \text{Im} G(\mathbf{k}, \omega + i0^+). \quad (19)$$

This is a central observable which is related, for $\omega < 0$, to the \mathbf{k} -resolved (angle-resolved) photoemission spectrum (PES), and, for $\omega > 0$, to the inverse photoemission spectrum (inverse photoemission, IPE). PES and IPE probe the occupied and the unoccupied part of the electronic

structure in the vicinity of the Fermi energy ($\omega = 0$), respectively. With the help of the Dirac identity, $\lim_{\eta \searrow 0} 1/(x + i\eta) = \mathcal{P}(1/x) - i\pi\delta(x)$, we also have the expression

$$A_{\mathbf{R},\mathbf{R}'}(\omega) = \left\langle 0 \left| c_{\mathbf{R}',\sigma}^\dagger \delta(\omega - E_0 + H) c_{\mathbf{R},\sigma} \right| 0 \right\rangle + \left\langle 0 \left| c_{\mathbf{R},\sigma} \delta(\omega + E_0 - H) c_{\mathbf{R}',\sigma}^\dagger \right| 0 \right\rangle \quad (20)$$

for real ω , and

$$G_{\mathbf{R},\mathbf{R}'}(\omega) = \int_{-\infty}^{\infty} d\omega' \frac{A_{\mathbf{R},\mathbf{R}'}(\omega')}{\omega - \omega'} . \quad (21)$$

The simplest case is that of a noninteracting tight-binding model with Hamiltonian

$$H_0 = \sum_{\mathbf{R}\mathbf{R}'\sigma} t_{\mathbf{R}\mathbf{R}'} c_{\mathbf{R}\sigma}^\dagger c_{\mathbf{R}'\sigma} . \quad (22)$$

Expressing the δ -function in Eq. (20) as $\delta(\omega) = (2\pi)^{-1} \int dt e^{-i\omega t}$, using the Baker-Campbell-Hausdorff formula, $e^B A e^{-B} = e^{-L_B} A$ for operators A, B and $L_B A \equiv [A, B]$, and the elementary commutator $[c_{\mathbf{R}\sigma}, H_0] = \sum_{\mathbf{R}'} t_{\mathbf{R},\mathbf{R}'} c_{\mathbf{R}'\sigma}$, we find

$$\mathbf{A}(\omega) = \delta(\omega - \mathbf{t}) , \quad A(\mathbf{k}, \omega) = \delta(\omega - \epsilon(\mathbf{k})) , \quad (23)$$

where $\epsilon(\mathbf{k})$ are the eigenvalues of the hopping matrix \mathbf{t} , i.e., the tight-binding dispersion. Here, we discuss the case of electrons on a two-dimensional square lattice with hopping between nearest neighbors only, i.e., $t_{\mathbf{R},\mathbf{R}'} = -t$ if \mathbf{R}, \mathbf{R}' are nearest-neighbor sites. $t = 1$ fixes the energy scale. The dispersion is obtained by lattice Fourier transformation, $\epsilon(\mathbf{k}) \delta_{\mathbf{k}\mathbf{k}'} = (\mathbf{U}^\dagger \mathbf{t} \mathbf{U})_{\mathbf{k}\mathbf{k}'}$, with

$$\epsilon(\mathbf{k}) = -2t(\cos k_x + \cos k_y) . \quad (24)$$

With this we obtain the noninteracting spectral density as displayed in Fig. 3 (left). $A(\mathbf{k}, \omega)$ has exactly one δ -singularity for each \mathbf{k} in the reciprocal unit cell, e.g., in the first Brillouin zone. There is a well-defined Fermi surface, given by all \mathbf{k} -points in the BZ with vanishing excitation energy: $\omega = \epsilon(\mathbf{k}) = 0$. The band is half-filled. Different band fillings are obtained by introducing a chemical potential $\mu \neq 0$ via the substitution $H_0 \mapsto H_0 - \mu N$, where N is the particle-number operator.

The *interacting* spectral density Fig. 3 (right) looks quite different. The example shows $A(\mathbf{k}, \omega)$ for the same tight-binding model but with an additional on-site Coulomb interaction

$$H_1 = \frac{U}{2} \sum_{\mathbf{R}\sigma} n_{\mathbf{R}\sigma} n_{\mathbf{R}-\sigma} \quad (25)$$

of strength U , where $n_{\mathbf{R}\sigma} \equiv c_{\mathbf{R}\sigma}^\dagger c_{\mathbf{R}\sigma}$ is the occupation-number operator. $H = H_0 + H_1$ is the famous Hubbard model [18–20] which frequently serves as a prototype for method developments. The computation of the spectral density in the interacting cases is, of course, by no means trivial. The example shown here displays quantum Monte-Carlo data for the Hubbard model on $L = L_x \times L_y = 64$ sites from a study performed about 20 years ago [21]. Since then we have seen various improvements of the QMC method but the infamous sign problem, which prevents an efficient simulation of the model off half-filling, for example, is still unsolved in

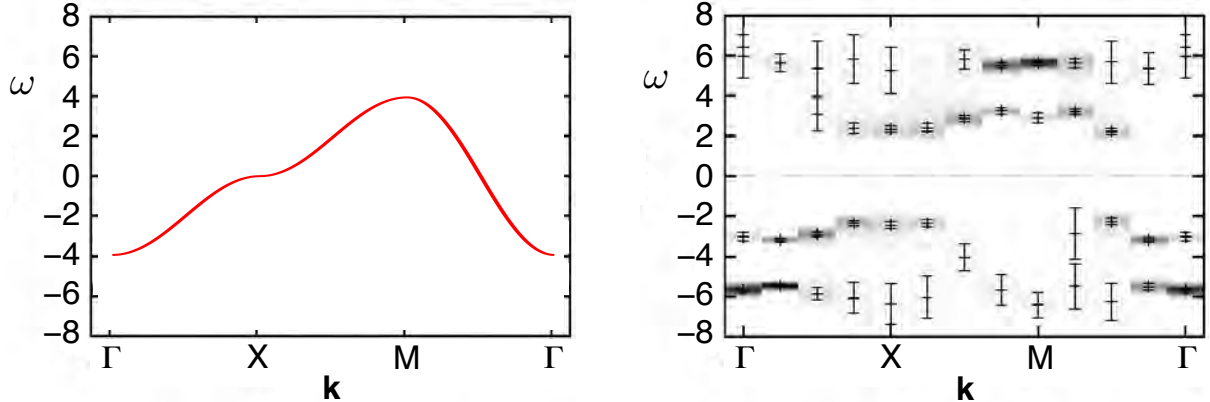


Fig. 3: Spectral function $A(\mathbf{k}, \omega)$ for the two-dimensional Hubbard model at half-filling along high-symmetry paths in the first Brillouin zone. $\Gamma = (0, 0)$, $X = (\pi, 0)$, $M = (\pi, \pi)$. The nearest-neighbor hopping is set to $t = 1$. Left: Result for $U = 0$. Here, $A(\mathbf{k}, \omega) = \delta(\omega - \epsilon(\mathbf{k}))$, where $\epsilon(\mathbf{k})$ is the tight-binding dispersion. Right: Quantum Monte-Carlo result for $U = 8$. Figure adapted from Refs. [21, 22].

general. At half-filling, however, the lattice QMC approach is very powerful. This is obvious when comparing to exact diagonalization (ED) techniques, for example, which suffer from the exponentially growing Hilbert-space with increasing system size. The enormous size of the Hilbert space dimension for $L = 64$ is way beyond what can be accessed by ED.

5 Local and nonlocal correlations

The results displayed in Fig. 3 have been computed for the Hubbard model at $U = 8$, i.e., $U = W$, where W is the width of the noninteracting band, and $\mu = U/2$, which enforces half-filling, and a high inverse temperature $\beta = 10$. The example is very instructive as it embodies a couple of famous many-body effects: First of all, it is obvious that the single-electron excitations are gapped in the interacting case; there is no finite spectral weight in the vicinity of $\omega = 0$ and thus no Fermi surface. This is a nice demonstration of Mott-insulating behavior, i.e., the system is an interaction-driven insulator. The standard explanation is that, for strong U , each site of the lattice is almost perfectly occupied by exactly one electron as the gain in kinetic energy $\sim t$ due to delocalization of the electrons in the ground state is much smaller than the energy penalty $\sim U$ that would have to be paid when double occupancies were created. An excitation of the ground state carrying charge must therefore bridge a large gap of the order of U . This explains the insulating character of the system.

Second, while there are well-defined and dispersing single-electron excitations visible, these are not δ -function-like but smeared out in energy to some degree. The intrinsic broadening of the excitations is in fact due to their decay as mediated by the interaction. This lifetime effect is clearly beyond the simple bandstructure picture. Quite generally, there are typically large ranges in the (\mathbf{k}, ω) -plane, where the spectral weight is finite but where there are no well-defined peaks. This “incoherent background” must be seen as the result of complicated decay products. The initial excitation of the system affects a single electron only. The remaining final state $c_{R\sigma}^{(\dagger)} |0\rangle$,

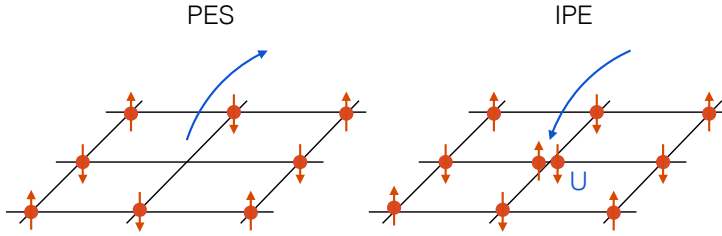


Fig. 4: Schematic representation of the high-energy single-electron excitations of the half-filled Hubbard model for strong U . The lower Hubbard band results from $\omega < 0$ (photoemission, PES) excitations leaving a hole in the final state which propagates through the lattice. The upper Hubbard band results from $\omega > 0$ (inverse photoemission, IPE) excitations leaving a propagating double occupancy in the final state.

however, is not an eigenstate. It may decay in a high-order process, involving high powers of H_0 and H_1 , into states with many low-energy excitations of many electrons. The phase space for such complex decay processes is not very much restricted by energy and momentum conservation, it is huge, and thus one would expect a broad and featureless continuum.

Third, there are still some well-defined structures with high spectral weight. For example, there are *two* “bands” with high spectral weight, one around Γ at negative frequencies $\omega \approx -6$ (PES) and another one around the M points at positive frequencies $\omega \approx +6$ (IPE), rather than a single band as in the $U = 0$ limit. These are the so-called lower (LHB) and upper Hubbard bands (UHB), see Fig. 4. They are related to each other via the general constraint $A(\mathbf{k}, \omega) = A(\mathbf{k} + \mathbf{Q}, -\omega)$ with $\mathbf{Q} = (\pi, \pi)$, which results from particle-hole symmetry present at half-filling and a bipartite lattice with nearest-neighbor hopping. Note that the bandstructure paradigm cannot explain those “bands”: Irrespective of the form of H_0 , there is exactly one (δ -like) peak per \mathbf{k} -point on the ω axis. One therefore speaks about correlation-induced *satellites*. Physically, the lower Hubbard band results from the propagation of the hole in the final state of the electron-removal (photoemission) process. In the $U \rightarrow \infty$ limit we expect that the final-state hole propagates almost freely through the lattice, such that a dispersive structure with spectral width of $W_{\text{LHB}} = 8$ is generated. An analogous explanation holds for the upper Hubbard band seen in IPE. Here, the electron-addition (inverse photoemission) process produces an itinerant doubly occupied site in the final state resulting in a dispersive excitation with $W_{\text{UHB}} = 8$ for strong U . The excitation energies can be read off from Eq. (20) (however, one has to include the μ -shift in addition): The lower Hubbard band is centered around $\omega = E_0 - E_n - \mu \approx -\mu = -U/2$ while the upper Hubbard band lies at $\omega = E_n - E_0 - \mu \approx U - \mu = +U/2$, such that their energy difference, the Hubbard gap, is given by $\Delta_{\text{UHB-LHB}} \approx U$ for $U \rightarrow \infty$. Apart from their dispersion, the existence of the Hubbard bands is due to a local effect, namely due to the local charge correlation at the site where the (inverse) photoemission process takes place. Hubbard bands are said to be an effect of *local correlations*.

Besides the Hubbard bands at high excitation energies, there are rather well-defined low-energy structures in the spectrum at $\omega \approx \pm 3$. These result from *nonlocal correlations*, in particular from nonlocal antiferromagnetic correlations, as is explained by the superexchange mechanism, see Fig. 5: Recall that for strong U , the occupancy of each site is almost unity in the ground

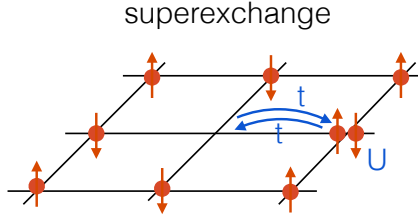


Fig. 5: Superexchange mechanism in the Hubbard model at half-filling and for strong U . See text for explanation.

state of the system. If the occupancy was perfectly unity, the ground state would have a macroscopic 2^L -fold degeneracy as each localized electron corresponds to a local spin-1/2. The true ground state, however, has a small but important admixture of configurations with somewhat delocalized electrons. These result from the fact that the ground-state energy can be lowered by a second-order hopping process gaining delocalization energy, while a double occupancy is merely created virtually. Due to the Pauli principle, however, such superexchange processes are only possible, if neighboring spins align antiferromagnetically. Hence, the ground state is a nondegenerate singlet in which neighboring local spins

$$s_R \equiv \frac{1}{2} \sum_{\sigma\sigma'} c_{R\sigma}^\dagger \boldsymbol{\tau}_{\sigma\sigma'} c_{R\sigma'} \quad (26)$$

($\boldsymbol{\tau} = (\sigma_x, \sigma_y, \sigma_z)$ is the vector of Pauli matrices) are antiferromagnetically correlated. In fact, using strong-coupling perturbation theory at second order in t/U , one can map the low-energy sector of the Hubbard model onto the spin-1/2 Heisenberg model with antiferromagnetic exchange interaction $J = 4t^2/U$ [23]. Hence, the *low-energy* excitations of the Hubbard model are nonlocal spin excitations with a band width of about $2J$ (with $2J = 1$ at $U = 8$). These spin excitations couple to the single-electron excitations, they “dress” the moving hole (PES) or the moving doublon (IPE), i.e., the hole / doublon constantly emits and reabsorbs spin excitations during its motion through the antiferromagnetic spin structure. This gives rise to a renormalization of the Hubbard “bands” but also to novel structures in $A(\mathbf{k}, \omega)$ at low frequencies (here, at intermediate U , at $\omega \approx \pm 3$) which must be seen as fingerprints of nonlocal antiferromagnetic correlations.

Much higher resolution would be necessary to get still deeper insight into the physics of the model. Resolution is limited, however, by various factors: (i) The finite lattice size leads to an artificial discretization of \mathbf{k} -space. With $L = 64$, as in the present example, the spacing between \mathbf{k} -points along Γ - X , i.e., along the k_x -line in the BZ ($-\pi < k_x < \pi$) is $\Delta k_x = 2\pi/8$; there are 4 \mathbf{k} -points only between Γ and X . (ii) The QMC calculations must be run at finite temperatures. Here, the inverse temperature is $\beta = 10$ which already has some unwanted impact, such as thermal broadening and thermally induced decay of correlations. (iii) For technical reasons, QMC is implemented on the imaginary time (τ) axis. Data obtained for $A(\mathbf{k}, \tau)$ must be extrapolated, using the maximum-entropy method, for instance, to the real-frequency axis. This produces an additional unwanted broadening of spectral structures.

6 Cluster perturbation theory

Roughly, DMFT treats local correlations correctly but is not able to account for the effects of nonlocal correlations. The importance of the latter is a strong motivation to construct cluster extensions of the DMFT. To develop the main ideas and to get first insights, we will start with a much simpler approach, namely with the cluster perturbation theory (CPT) [24, 25].

Consider again the simple noninteracting tight-binding model H_0 , as given by Eq. (22). The left diagram in Fig. 6 represents H_0 for the two-dimensional case and for hopping between nearest neighbors only. Next, we consider a model which is obtained from H_0 by grouping the L sites of the lattice into L/L_c identical clusters consisting of L_c sites each and by neglecting the hopping between the clusters, see Fig. 6 (middle). The corresponding Hamiltonian is

$$H'_0 = \sum_{\mathbf{R}_1 \mathbf{R}_2 \sigma} t'_{\mathbf{R}_1, \mathbf{R}_2} c_{\mathbf{R}_1 \sigma}^\dagger c_{\mathbf{R}_2 \sigma}. \quad (27)$$

This system is called the *reference system* opposed to the *original system* with Hamiltonian H_0 . If \mathbf{t} with elements $t_{\mathbf{R}_1, \mathbf{R}_2}$ is the hopping matrix of the original system, and \mathbf{t}' the hopping matrix of the reference system, then

$$\mathbf{V} = \mathbf{t} - \mathbf{t}' \quad (28)$$

is the neglected inter-cluster hopping, see Fig. 6, right. Obviously, the translation symmetry group of H'_0 is described by a superlattice.

The Green function of the model H_0 is

$$\mathbf{G}_0(\omega) = \frac{1}{\omega + \mu - \mathbf{t}}. \quad (29)$$

Here, we have explicitly introduced the chemical potential μ (which is not important here but will be used later). Furthermore, we again employ a matrix notation and write ω rather than $\omega \mathbf{1}$ for short etc. Note that $(\cdots)^{-1}$ and $1/(\cdots)$ mean matrix inversion.

The reference system's Green function is

$$\mathbf{G}'_0(\omega) = \frac{1}{\omega + \mu - \mathbf{t}'} . \quad (30)$$

In this case the matrix inverse is in a way simpler to compute since the hopping matrix \mathbf{t}' has a block structure as it does not connect sites in different clusters. Therefore, the following question comes up: Having the Green function of the reference system at hand, how can we get the Green function of the original model H_0 ? With some algebra, one easily derives the equation

$$\mathbf{G}_0(\omega) = \mathbf{G}'_0(\omega) + \mathbf{G}'_0(\omega) \mathbf{V} \mathbf{G}_0(\omega), \quad (31)$$

which is solved by

$$\mathbf{G}_0(\omega) = \frac{1}{\mathbf{G}'_0(\omega)^{-1} - \mathbf{V}} . \quad (32)$$

We see that using Green functions it is formally rather easy to couple a system of isolated clusters. For the noninteracting system this is not of much importance. In particular, in Eq. (32) the block structure is lost when adding $-\mathbf{V}$ to $\mathbf{G}'_0(\omega)^{-1}$.

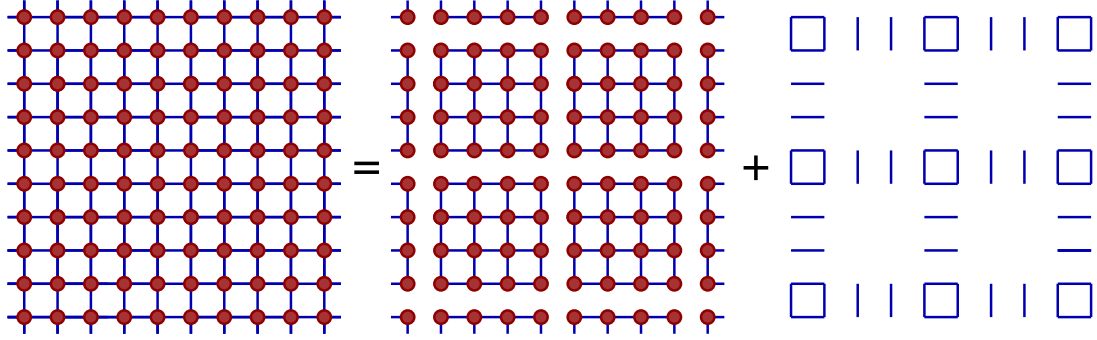


Fig. 6: Left: Graphical representation of a tight-binding model with hopping between nearest neighbors on a square lattice. Hopping matrix t . Middle: The same model but with vanishing hopping between identical clusters consisting of $L_c = 16$ sites each. Hopping matrix t' . Right: The neglected inter-cluster hopping V . Taken from Ref. [26].

However, we are actually interested in interacting systems. Let us, therefore, take the Hubbard model as our original system $H = H_0 + H_1$ with the interaction term given by Eq. (25). The reference model shall again be defined by switching off the inter-cluster hopping V . Its Hamiltonian is $H' = H_0(t') + H_1$. Note that since H_1 consists of completely local terms, the reference system consists of a set of interacting but decoupled clusters. Therefore, it is comparatively easy to solve the problem exactly (by numerical means if necessary), while for the original lattice model this is a hard problem. Of course, there is no simple relation between the Green functions of the original and of the reference system like Eq. (31). Nevertheless, it is very tempting to assume that $\mathbf{G}(\omega)$ satisfies

$$\mathbf{G}(\omega) = \mathbf{G}'(\omega) + \mathbf{G}'(\omega) \mathbf{V} \mathbf{G}(\omega), \quad (33)$$

where both \mathbf{G} and \mathbf{G}' are interacting Green functions. This equation constitutes the cluster perturbation theory [24, 25]. The CPT provides an approximate expression for \mathbf{G} which is easy to compute (numerically) if L_c is not too large.

There is an independent and equivalent way to motivate the CPT: It starts from the Dyson equation for the reference system

$$\mathbf{G}'(\omega) = \mathbf{G}'_0(\omega) + \mathbf{G}'_0(\omega) \boldsymbol{\Sigma}'(\omega) \mathbf{G}'(\omega), \quad (34)$$

which may be solved for the self-energy, i.e., $\boldsymbol{\Sigma}'(\omega) = \mathbf{G}'_0(\omega)^{-1} - \mathbf{G}'(\omega)^{-1}$. Assuming that $\boldsymbol{\Sigma}'(\omega)$ is a good approximation for the self-energy of the original system,

$$\boldsymbol{\Sigma}(\omega) \approx \boldsymbol{\Sigma}'(\omega), \quad (35)$$

and inserting into the Dyson equation of the original system,

$$\mathbf{G}(\omega) = \mathbf{G}_0(\omega) + \mathbf{G}_0(\omega) \boldsymbol{\Sigma}(\omega) \mathbf{G}(\omega), \quad (36)$$

immediately yields the CPT equation (33) when using Eqs. (29) and (30).

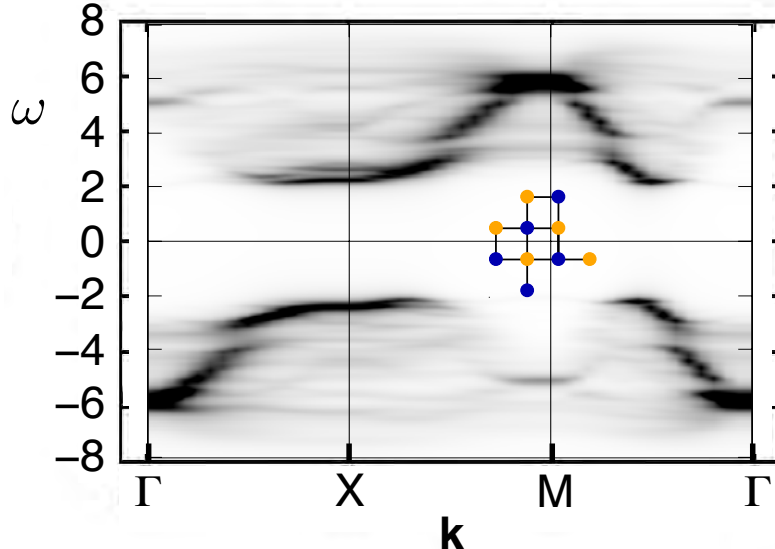


Fig. 7: The same as in Fig. 3 for $U = 8$ but results are obtained with the CPT using $L_c = 10$ -site clusters. See inset for cluster geometry. Figure adapted from Ref. [22].

The idea to approximate the self-energy by the self-energy of the reference system is motivated by the fact that the self-energy of the Hubbard model or, more generally, of models with local interactions, is a quantity that is “more local” than the Green function. In the limit of a high-dimensional hypercubic lattice with nearest-neighbor hopping $t_{RR'} = \text{const}/D^{1/2}$, for example, the nearest-neighbor elements of the self-energy scale as $\Sigma_{RR'\sigma}(\omega) \sim 1/D^{3/2}$ while $G_{RR'\sigma}(\omega) \sim 1/D^{1/2}$ [4]. While the CPT is a systematic approximation, which is controlled by the size of the clusters in the reference system and which trivially becomes exact in the infinite-cluster limit $L_c \rightarrow \infty$, it must be seen as a comparatively crude approximation for typical cluster sizes used in practice, see Ref. [27] and references therein, for instance. For cluster size $L_c = 1$ it reduces to the simple Hubbard-I approximation. Still, the CPT can provide us with a rather good first idea about the Green function and the spectral density. This is demonstrated with Fig. 7 which shows the spectral density of the Hubbard model, as in Fig. 3, but obtained by CPT for clusters with $L_c = 10$ sites. The cluster geometry is shown in the inset. One can easily see that this can be used for a tiling of the two-dimensional square lattice. As a rule of thumb, compact but asymmetric cluster shapes are preferable. Indeed, the CPT result quite nicely reproduces the results of the much more elaborate QMC approach.

7 Periodization schemes

There is an obvious problem, which is actually shared by any cluster approach that is formulated in real space. Namely, as the reference system is given by a set of decoupled clusters, the approximate self-energy does not preserve the translational symmetries of the original lattice. The CPT Green function $G_{R,R'}(\omega) = G_{\tilde{R}\tilde{R}',rr'}(\omega)$ is merely invariant under superlattice translations $\tilde{R} \rightarrow \tilde{R} + \Delta\tilde{R}$. (Note that we use a notation with the spin-projection index σ suppressed). This means $G_{\tilde{R}\tilde{R}',rr'}(\omega) = G_{\tilde{R}+\Delta\tilde{R},\tilde{R}'+\Delta\tilde{R},r,r'}(\omega)$. Hence, Fourier transformation

\mathbf{V} , see Eq. (12), diagonalizes \mathbf{G} with respect to the superlattice indices

$$\frac{L_c}{L} \sum_{\tilde{\mathbf{R}}\tilde{\mathbf{R}'}} V_{\tilde{\mathbf{k}},\tilde{\mathbf{R}}}^\dagger G_{\tilde{\mathbf{R}}\tilde{\mathbf{R}'},rr'}(\omega) V_{\tilde{\mathbf{R}'},\tilde{\mathbf{k}'}} = G_{rr'}(\tilde{\mathbf{k}},\omega) \delta_{\tilde{\mathbf{k}}\tilde{\mathbf{k}'}} \quad (37)$$

with

$$G_{rr'}(\tilde{\mathbf{k}},\omega) = \left(\frac{1}{\omega + \mu - \mathbf{t}(\tilde{\mathbf{k}}) - \Sigma(\omega)} \right)_{rr'}. \quad (38)$$

Here, the V -Fourier transform $\mathbf{t}(\tilde{\mathbf{k}})$ of the hopping matrix $t_{\tilde{\mathbf{R}}\tilde{\mathbf{R}'},rr'}$ is an $L_c \times L_c$ matrix with elements $t_{rr'}(\tilde{\mathbf{k}})$ for each wave vector $\tilde{\mathbf{k}}$ in the reciprocal supercell. The self-energy is “cluster-local”, i.e., it is diagonal in the superlattice indices $\tilde{\mathbf{R}}, \tilde{\mathbf{R}'}$, and thus, after V -Fourier transformation, is independent of $\tilde{\mathbf{k}}$. The “cluster-local” elements of \mathbf{G} with $\tilde{\mathbf{R}} = \tilde{\mathbf{R}'}$ are obtained by

$$G_{rr'}^{(\text{loc})}(\omega) = \frac{L_c}{L} \sum_{\tilde{\mathbf{k}} \in \mathcal{RSC}} \left(\frac{1}{\omega + \mu - \mathbf{t}(\tilde{\mathbf{k}}) - \Sigma(\omega)} \right)_{rr'}. \quad (39)$$

From the fully local elements $G_{rr}^{(\text{loc})}(\omega)$ we then get the local interacting density of states (LDOS) at a site $\mathbf{R} = (\tilde{\mathbf{R}}, \mathbf{r})$ as

$$A_{\mathbf{R}}(\omega) = -\frac{1}{\pi} \text{Im} G_{rr}(\omega + i0^+). \quad (40)$$

One would expect that the LDOS exhibits the same (translational) symmetries as the Hamiltonian of the original system and of the original lattice: $A_{\mathbf{R}}(\omega) = A(\omega)$. Within the CPT, however, there is an artificial dependence of the LDOS on \mathbf{r} .

A modified cluster-perturbation theory, constructed in the same way as the standard CPT but considering periodic boundary conditions for each of the individual clusters, has been suggested by Zacher *et al.* [28]. It has been recognized [29], however, that this gives less convincing results in practice. The modified CPT makes the Green function invariant under translations within each cluster. However, since $\mathbf{U} \neq \mathbf{VW}$, there is also no improvement on the formal level.

One could also try to transform the original model and the reference system as well to reciprocal space. This straightforward idea means to express H and H' in terms of annihilators $c_{\mathbf{k}}$ rather than $c_{\mathbf{R}}$ and analogously for the creators and to employ the CPT decoupling thereafter. Clearly, H' will exhibit the full translational symmetry. However, the idea will not work for models with local interactions, such as the Hubbard model. A local interaction in real space transforms into a delocalized one in \mathbf{k} -space where the interaction parameters $U_{\mathbf{k}\mathbf{k}'\mathbf{k}''\mathbf{k}''}$ basically couple any \mathbf{k} point to any other.

With respect to the local spectral density (40), a pragmatic way out would be to average over the cluster sites

$$A(\omega) \equiv \frac{1}{L_c} \sum_{\mathbf{r}} A_{(\tilde{\mathbf{R}}, \mathbf{r})}(\omega) = \frac{1}{L} \sum_{\mathbf{R}} A_{\mathbf{R}}(\omega). \quad (41)$$

One thus distinguishes between the CPT spectral density on the one hand and the translationally invariant (“physical”) spectral density on the other. Generally, a periodization operator \widehat{T} can be defined which, for example, enforces a translationally invariant Green function: $\mathbf{G}(\omega) \mapsto \widehat{T}[\mathbf{G}](\omega)$. A possible construction of \widehat{T} is to start with a U -Fourier transform of the CPT Green function from \mathbf{R} -space to \mathbf{k} -space. As the Green function does not fully respect the translation symmetries, this transformation does not fully diagonalize the Green function, and we get $G_{\mathbf{k}\mathbf{k}'}(\omega)$ with nonzero elements for $\mathbf{k} \neq \mathbf{k}'$. Periodization is then achieved by replacing $G_{\mathbf{k}\mathbf{k}'}(\omega) \mapsto G_{\mathbf{k}\mathbf{k}}(\omega) \delta_{\mathbf{k},\mathbf{k}'} \equiv \widehat{T}[\mathbf{G}]_{\mathbf{k}\mathbf{k}'}(\omega)$. This provides us with a translationally invariant (physical) Green function $\widehat{T}[\mathbf{G}](\omega)$. In real space, this periodization reads

$$\widehat{T}[\mathbf{G}]_{\mathbf{R}\mathbf{R}'} = \frac{1}{L} \sum_{\mathbf{R}''\mathbf{R}'''} \delta_{\mathbf{R}-\mathbf{R}',\mathbf{R}''-\mathbf{R}'''} G_{\mathbf{R}''\mathbf{R}'''} . \quad (42)$$

For $\mathbf{R} = \mathbf{R}'$, in particular, we have

$$\widehat{T}[\mathbf{G}]_{\mathbf{R}\mathbf{R}}(\omega) = \frac{1}{L} \sum_{\mathbf{R}''\mathbf{R}'''} \delta_{\mathbf{R}''\mathbf{R}'''} G_{\mathbf{R}''\mathbf{R}'''}(\omega) = \frac{1}{L} \sum_{\mathbf{R}} G_{\mathbf{R}\mathbf{R}}(\omega) = \frac{1}{L_c} \sum_{\mathbf{r}} G_{\mathbf{r}\mathbf{r}}(\omega), \quad (43)$$

consistent with Eq. (41). This periodization is actually a standard procedure and has also been used to produce the results displayed in Fig. 7. In addition a smoothening of the spectrum has been employed by replacing the positive infinitesimal 0^+ with a small but finite value $\eta > 0$ in Eq. (19). This is necessary since the Green function of the reference system and thus the CPT self-energy consists of a finite number of poles only such that, even after periodization Eq. (41), the LDOS is composed of a finite number of δ -peaks only.

A different periodization scheme is given by periodizing the CPT self-energy,

$$\boldsymbol{\Sigma}(\omega) \mapsto \widehat{T}[\boldsymbol{\Sigma}](\omega) . \quad (44)$$

Concretely, with $\Sigma_{(\tilde{\mathbf{R}},\mathbf{r}),(\tilde{\mathbf{R}}',\mathbf{r}')}(\omega) = \Sigma_{\mathbf{r},\mathbf{r}'}(\omega) \delta_{\tilde{\mathbf{R}},\tilde{\mathbf{R}}'}$, we have

$$\widehat{T}[\boldsymbol{\Sigma}]_{(\tilde{\mathbf{R}},\mathbf{r}),(\tilde{\mathbf{R}}',\mathbf{r}')}(\omega) = \frac{1}{L_c} \sum_{\mathbf{r}'',\mathbf{r}'''} \delta_{\tilde{\mathbf{R}}+\mathbf{r}-\tilde{\mathbf{R}}'-\mathbf{r}',\mathbf{r}''-\mathbf{r}'''} \Sigma_{\mathbf{r}'',\mathbf{r}'''}(\omega) . \quad (45)$$

This produces a self-energy which fully respects the translational symmetries and thus, via Eq. (36), a fully translationally invariant Green function. Both periodization schemes share the same *ad hoc* character. The periodization of the self-energy appears a bit more artificial, as the necessary *ad hoc* approximation is performed at an earlier stage of the theory rather than at the very end.

Note that any periodization scheme can also be used to restore point-group symmetries of the original lattices which are usually violated by the plain CPT as well. Fig. 8 gives some examples for various cluster sizes. In most cases, and already for $L_c = 2$, the reference system has a lower point-group symmetry. The periodization operator, Eq. (42), can be seen as an average over all possible translations. In basically the same way, by properly generalizing the operator \widehat{T} , one can restore not only the translational but also the discrete rotational and reflection symmetries.

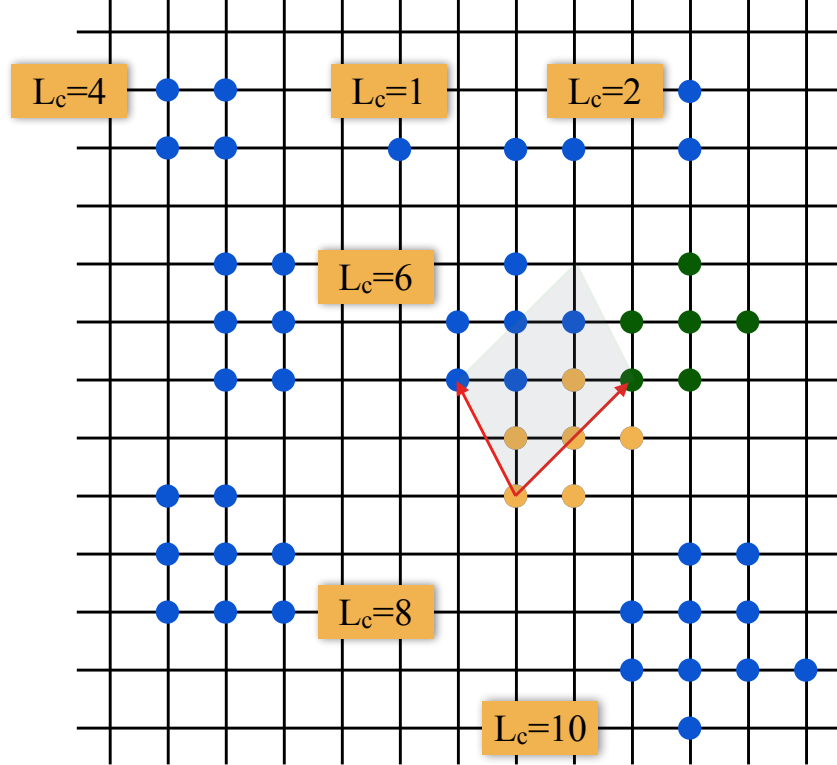


Fig. 8: Different tilings of the square lattice into clusters with L_c sites each. See text for discussion.

A completely different idea to generate a CPT-based approximation respecting the discrete symmetries is the “periodic CPT” which has been suggested by Tran Minh-Tien [30] and which is inspired by the dynamical cluster approximation (DCA) discussed below. Here, one modifies the hopping matrix of the *original system*, $t \mapsto \bar{t}$, rather than the hopping of reference system t' . The latter is still taken as a system consisting of identical isolated clusters but with periodic boundary conditions for each individual cluster. For a one-dimensional system, Fig. 9 illustrates the hopping matrix of the original system (a) and of the reference system (b). The symmetries of the latter are given by (i) the intra-cluster translations \mathbf{r} and by (ii) the superlattice translations $\tilde{\mathbf{R}}$. Now, the construction of \bar{t} is such that it exhibits the same translational symmetries. Consider a cluster translation $(\tilde{\mathbf{R}}, \mathbf{r}) \mapsto (\tilde{\mathbf{R}}, \mathbf{r} + \Delta\mathbf{r})$ with $\Delta\mathbf{r}$ connecting nearest neighbors in a cluster (with periodic boundary conditions on the cluster). The corresponding transformation of the hopping amplitudes of the reference system is a symmetry: $t'_{\tilde{\mathbf{R}}, \mathbf{r}, \tilde{\mathbf{R}}', \mathbf{r}'} \mapsto t'_{\tilde{\mathbf{R}}, \mathbf{r} + \Delta\mathbf{r}, \tilde{\mathbf{R}}', \mathbf{r}' + \Delta\mathbf{r}} = t'_{\tilde{\mathbf{R}}, \mathbf{r}, \tilde{\mathbf{R}}', \mathbf{r}'}$. To make it a symmetry of the hopping of the original system as well, some hopping amplitudes must be added. Panel (c) of the figure gives an example for a specific nearest-neighbor cluster translation which is equivalent with a cyclic permutation of the sites within each cluster. The upper part shows the hopping amplitudes present in t , while the lower one shows those that are generated by the translation. The hopping amplitudes generated by all cluster translations are included in the new hopping matrix \bar{t} , see panel (d).

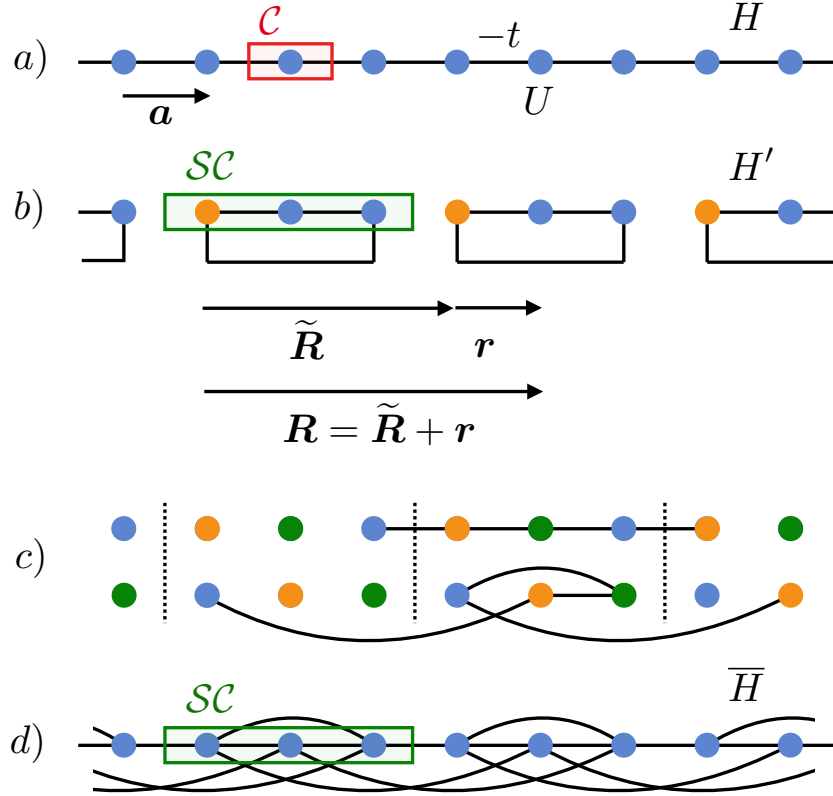


Fig. 9: Construction of the modified original system \bar{H} for a one-dimensional lattice. a) Original system H , black lines: nearest-neighbor hopping $-t$, on-site Hubbard interaction U , unit cell C . b) Reference system H' : superlattice (basis) vector \tilde{R} , cluster vector r , supercell SC with $L_c = 3$ (cf. Fig. 2). c) A cyclic permutation of the sites within each cluster is a symmetry of H' . Black lines in the upper panel: nearest-neighbor hopping parameters related to a given cluster. Lower panel: resulting hopping parameters after the transformation. d) Hopping parameters of the Hamiltonian \bar{H} , which is invariant (i) under all intra-cluster translations and (ii) under all superlattice translations.

Note that for $L_c \rightarrow \infty$ the inclusion of the additional hopping amplitudes becomes irrelevant. Hence, the replacement $\mathbf{t} \mapsto \bar{\mathbf{t}}$ is controlled by L_c , i.e., it becomes exact, up to irrelevant boundary terms, in the infinite-cluster limit. The explicit construction of $\bar{\mathbf{t}}$ is the following

$$\bar{\mathbf{t}} = (\mathbf{V}\mathbf{W})\mathbf{U}^\dagger \mathbf{t} \mathbf{U}(\mathbf{V}\mathbf{W})^\dagger. \quad (46)$$

Let us stress once more, that $\mathbf{V}\mathbf{W} \neq \mathbf{U}$ for clusters of finite size L_c . The first transformation $\mathbf{U}^\dagger \mathbf{t} \mathbf{U}$ diagonalizes the hopping matrix \mathbf{t} , and the diagonal elements are given by $\varepsilon(\mathbf{k}) = \varepsilon(\tilde{\mathbf{G}} + \tilde{\mathbf{k}})$ with a uniquely defined reciprocal superlattice vector $\tilde{\mathbf{G}}$ and a uniquely defined wave vector $\tilde{\mathbf{k}} \in \mathcal{R}SC$. Double back transformation using \mathbf{V} and \mathbf{W} then yields:

$$\bar{\mathbf{t}}_{RR'} = t_{\tilde{R},r;\tilde{R}',r'} = \frac{1}{L_c} \sum_{\tilde{\mathbf{G}}} e^{i\tilde{\mathbf{G}}(r-r')} \frac{L_c}{L} \sum_{\tilde{\mathbf{k}}} e^{i\tilde{\mathbf{k}}(\tilde{R}-\tilde{R}')} \varepsilon(\tilde{\mathbf{k}} + \tilde{\mathbf{G}}). \quad (47)$$

Obviously, $\bar{\mathbf{t}}$ is invariant under both, superlattice translations as well as cluster translations.

Applying CPT to the original system Fig. 9(d) using the reference system Fig. 9(b) yields

$$\mathbf{G}(\omega) = \frac{1}{\omega + \mu - \bar{\mathbf{t}} + \Sigma(\omega)} . \quad (48)$$

As the self-energy is taken from the reference system, it is diagonal with respect to superlattice translations $\tilde{\mathbf{R}}$ and is $\tilde{\mathbf{R}}$ -independent. Since the original as well as the reference system share the same symmetries both, $\Sigma(\omega)$ and $\bar{\mathbf{t}}$ are diagonalized by $\mathbf{V}\mathbf{W}$

$$G(\tilde{\mathbf{k}} + \tilde{\mathbf{G}}, \omega) = \frac{1}{\omega + \mu - \varepsilon(\tilde{\mathbf{k}} + \tilde{\mathbf{G}}) + \Sigma(\tilde{\mathbf{G}}, \omega)} . \quad (49)$$

Note that we have replaced the diagonal elements $\bar{\varepsilon}(\tilde{\mathbf{k}}, \tilde{\mathbf{G}})$ of $(\mathbf{V}\mathbf{W})^\dagger \bar{\mathbf{t}} (\mathbf{V}\mathbf{W})$ by the diagonal elements $\varepsilon(\tilde{\mathbf{k}} + \tilde{\mathbf{G}})$ of $\mathbf{U}^\dagger \mathbf{t} \mathbf{U}$, which becomes correct for $L_c \rightarrow \infty$ as discussed above. Likewise, again using the unique decomposition $\mathbf{k} = \tilde{\mathbf{k}} + \tilde{\mathbf{G}}$, we interpret $G(\tilde{\mathbf{k}} + \tilde{\mathbf{G}}, \omega) \equiv G(\tilde{\mathbf{k}}, \tilde{\mathbf{G}}, \omega)$ as $G(\mathbf{k}, \omega)$, i.e., as the diagonal elements of $\mathbf{U}^\dagger \mathbf{G}(\omega) \mathbf{U}$. In this way we have achieved our goal, and we get a CPT Green function respecting the full translational symmetries of the original lattice. Obviously, the periodized CPT (P-CPT) employs an implicit periodization scheme, which is approximate for any finite L_c but becomes exact, as the CPT approximation itself, in the $L_c \rightarrow \infty$ limit. We note that for finite L_c , the \mathbf{k} -dependence of the self-energy is discontinuous: $\Sigma(\tilde{\mathbf{k}} + \tilde{\mathbf{G}}) = \Sigma(\tilde{\mathbf{G}})$ is $\tilde{\mathbf{k}}$ -independent, i.e., within each of the L_c “patches” \mathcal{RSC} of the full reciprocal unit cell \mathcal{RC} of the original lattice, the self-energy is constant, while it jumps when crossing the boundaries between the patches. This unphysical feature of the P-CPT must be tolerated.

8 Self-consistent cluster-embedding approaches

A big disadvantage of the CPT and related cluster approximations is the lacking self-consistency. Let us recall that a generic mean-field theory not only takes a local perspective and focusses on a single site or on a small cluster cut out of an infinite lattice but also aims at a proper embedding of the site or the cluster in a mean field. The purpose of this mean field is to approximately account for the neglected environment of the cluster. The mean-field feeds back to the cluster problem but beyond that the quality of the mean-field theory improves considerably when the cluster observables feed back to the mean field as well, i.e., when cluster observables and mean field are determined self-consistently.

Table 2 gives an overview of various cluster approximations without (first column) and with self-consistent cluster embedding. Taking the self-energy of a single Hubbard site ($L_c = 1$),

$$\Sigma_{\mathbf{RR}'\sigma}(\omega) = \delta_{\mathbf{RR}'} U \langle n_{\mathbf{R}-\sigma} \rangle + \delta_{\mathbf{RR}'} \frac{U^2 \langle n_{\mathbf{R}-\sigma} \rangle (1 - \langle n_{\mathbf{R}-\sigma} \rangle)}{\omega + \mu - U(1 - \langle n_{\mathbf{R}-\sigma} \rangle)} , \quad (50)$$

as an approximation to compute the Green function for the Hubbard model is the essence of the Hubbard-I approximation. (Let us note that, in a strict sense, the Hubbard-I approximation does include some self-consistency and thus does not perfectly fit to the classification, see Ref. [18]).

impurity / cluster approaches		with self-consistent embedding	
Hubbard-I approach	[18]	DMFT	[1, 4]
CPT	[24, 25]	cellular DMFT (C-DMFT)	[9, 8]
simplified PC-DMFT		periodized C-DMFT	[31]
periodic CPT	[30]	DCA	[7]

Table 2: Different cluster approximations. See text for discussion.

The DMFT is a single-site mean-field theory as well ($L_c = 1$) but with a self-consistent embedding of the site. It is important to realize that this is a dramatic improvement. Even though the DMFT self-energy is local, $\Sigma_{RR'\sigma}(\omega) = \delta_{RR'} \Sigma_R(\omega)$, it has a realistic ω dependence with the typical branch cuts on the real axis rather than the simplistic single-pole structure of the Hubbard-I self-energy. The self-consistent DMFT embedding scheme is constructed such that one even recovers the exact solution of the Hubbard model in the limit, where the self-energy is local in fact [32], namely in the limit of infinite spatial dimensions [1].

Let us briefly recall the main idea for the Hubbard model as the original lattice model. To construct the single-site DMFT, we assume that the self-energy be local. In addition, a homogeneous (and nonmagnetic) phase is anticipated such that $\Sigma_{RR'\sigma}(\omega) = \delta_{RR'} \Sigma(\omega)$. We note in passing that this condition can be relaxed; this leads to real-space DMFT [33]. The most general reference system with a local self-energy and arbitrary ω -dependence is given by a single interacting (“impurity”) site with $U \neq 0$ hybridizing with a continuum of noninteracting bath degrees of freedom, i.e., by the single-impurity Anderson model

$$H' = \sum_{\sigma} \varepsilon_{\text{imp}} c_{\sigma}^{\dagger} c_{\sigma} + \frac{U}{2} \sum_{\sigma} n_{\text{imp},\sigma} n_{\text{imp},-\sigma} + \sum_{k\sigma} \varepsilon_k a_{k\sigma}^{\dagger} a_{k\sigma} + \sum_{k\sigma} \left(V_k c_{\sigma}^{\dagger} a_{k\sigma} + \text{H.c.} \right). \quad (51)$$

The local Green function on the impurity site is

$$G^{(\text{imp})}(\omega) = \frac{1}{\omega + \mu - \varepsilon_{\text{imp}} - \Delta(\omega) - \Sigma'(\omega)}. \quad (52)$$

The bath parameters, namely the hybridization strengths V_k and the on-site energies ε_k , enter the formalism via the hybridization function only:

$$\Delta(\omega) = \sum_k \frac{V_k^2}{\omega + \mu - \varepsilon_k}. \quad (53)$$

We will use the self-energy of the reference system as an approximation for the lattice model, $\Sigma(\omega) = \Sigma'(\omega)$. Obviously, a condition is needed to fix the hybridization function and therewith the parameters of the reference system. This self-consistency condition is obtained from the observation that the skeleton-diagram expansion leads to a functional relation between the self-energy and the Green function, $\Sigma = \widehat{\Sigma}[G]$, that is independent from the relation provided by the Dyson equation, see Fig. 10. On the single-site mean-field level or, equivalently, in the limit of infinite spatial dimensions, this functional is local, i.e., $\Sigma(\omega) = \widehat{\Sigma}[G^{(\text{loc})}](\omega)$ where

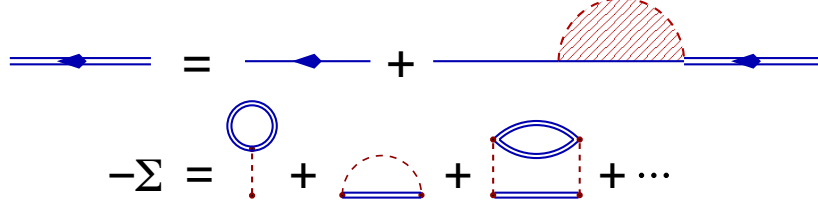


Fig. 10: Diagrammatic representation of the Dyson equation, $G(\omega) = G_0(\omega) + G_0(\omega)\Sigma(\omega)G(\omega)$ (top). Representation of the skeleton-diagram expansion of the self-energy, $\Sigma(\omega) = \widehat{\Sigma}[G](\omega)$ (bottom).

$G^{(\text{loc})}(\omega) = G_{RR}(\omega)$ is the local (on-site) element of the Green function. Hence, the functional relation $\widehat{\Sigma}[\dots]$ is exactly the same as that of the reference system: $\Sigma'(\omega) = \widehat{\Sigma}[G^{(\text{imp})}](\omega)$. With $\Sigma(\omega) = \Sigma'(\omega)$ this implies that

$$G^{(\text{imp})}(\omega) = G^{(\text{loc})}(\omega), \quad (54)$$

which is the famous self-consistency condition of DMFT.

The step from single-site DMFT to cellular DMFT is conceptually simple and corresponds to the step from the Hubbard-I approach to the CPT (see Tab. 2). One merely has to treat a finite Hubbard cluster with $L_c > 1$ sites as a “super site” and adopt the same strategy. The actual work to be done consists in the numerical computation of the self-energy $\Sigma'_{rr'}(\omega)$ of the Anderson “cluster” model

$$H' = \sum_{rr'\sigma} t_{rr'} c_{r\sigma}^\dagger c_{r'\sigma} + \frac{U}{2} \sum_{r\sigma} n_{r\sigma} n_{r-\sigma} + \sum_{k\sigma} \varepsilon_{rk} a_{rk\sigma}^\dagger a_{rk\sigma} + \sum_{rk\sigma} \left(V_{rk} c_{r\sigma}^\dagger a_{rk\sigma} + \text{H.c.} \right), \quad (55)$$

which is a small Hubbard model of L_c correlated sites, where each correlated site r hybridizes with an infinite number ($k = 1, \dots, \infty$) of bath sites. The $L_c \times L_c$ self-energy matrix is taken to approximate the “cluster local” self-energy of the Hubbard model, $\Sigma_{\tilde{R}\tilde{R},rr'}(\omega) = \Sigma'_{rr'}(\omega)$. With this at hand, one can compute the “cluster-local” elements of the Green function of the original model using the Dyson equation, cf. Eq. (39),

$$G_{rr'}^{(\text{loc})}(\omega) = \frac{L_c}{L} \sum_{\tilde{k} \in \mathcal{RSC}} \left(\frac{1}{\omega + \mu - \mathbf{t}(\tilde{\mathbf{k}}) - \boldsymbol{\Sigma}(\omega)} \right)_{rr'} \quad (56)$$

and therewith the cluster Green function of the reference system via the C-DMFT self-consistency equation $G_{rr'}^{(\text{cluster})}(\omega) = G_{rr'}^{(\text{loc})}(\omega)$. Using the cluster analog of Eq. (52), where $G^{(\text{imp})}(\omega)$ is replaced by the $L_c \times L_c$ matrix $\mathbf{G}^{(\text{cluster})}(\omega)$, $\Sigma'(\omega)$ by the matrix $\boldsymbol{\Sigma}(\omega)$, ε_{imp} by the $L_c \times L_c$ intra-cluster hopping matrix $\mathbf{t}' = \mathbf{t}$, and $\Delta(\omega)$ by the diagonal matrix $\boldsymbol{\Delta}(\omega)$, the diagonal elements of the latter are found as

$$\Delta_r(\omega) = \sum_{k\sigma} \frac{V_{rk}^2}{\omega + \mu - \varepsilon_{rk}} = \omega + \mu - t_{rr} - \Sigma_{rr}(\omega) - (\mathbf{G}^{(\text{cluster})})_{rr}^{-1}(\omega). \quad (57)$$

The parameters of the reference system (55) are obtained as the poles and the weights of $\Delta_r(\omega)$, such that an updated cluster self-energy can be computed. This self-consistency cycle must be iterated until convergence is achieved.

The C-DMFT does not respect the translational symmetries of the underlying lattice. One way to restore the correct symmetry is the so-called periodized C-DMFT (PC-DMFT) [31], see third row in Tab. 2. Here, one employs the periodization operator \widehat{T} to get a translationally invariant self-energy. The local Green function can thus be computed by U -Fourier transform and summation of \mathbf{k} . This yields the following PC-DMFT self-consistency equation:

$$G_{rr'}^{(\text{cluster})}(\omega) = G_{rr'}^{(\text{loc})}(\omega) = \frac{1}{L} \sum_{\mathbf{k}} \frac{e^{i\mathbf{k}(\mathbf{r}-\mathbf{r}')}}{\omega + \mu - \varepsilon(\mathbf{k}) - \widehat{T}[\Sigma](\mathbf{k}, \omega)}. \quad (58)$$

The main difference as compared to the C-DMFT, Eq. (56), is that the periodized self-energy is used at each step in the self-consistency cycle.

For the dynamical cluster approximation (DCA, fourth row in Tab. 2), one must replace the original hopping \mathbf{t} by $\bar{\mathbf{t}}$ only [31]. Both, \mathbf{t} and $\bar{\mathbf{t}}$, are invariant under superlattice translations. So we can compare $t_{rr'}(\tilde{\mathbf{k}}) = (\mathbf{V}^\dagger \mathbf{t} \mathbf{V})_{rr'}(\tilde{\mathbf{k}})$ with $\bar{t}_{rr'}(\tilde{\mathbf{k}}) = (\mathbf{V}^\dagger \bar{\mathbf{t}} \mathbf{V})_{rr'}(\tilde{\mathbf{k}})$. One easily finds that these are equal up to a phase factor

$$\begin{aligned} \bar{t}_{rr'}(\tilde{\mathbf{k}}) &= \frac{1}{L_c} \sum_{\tilde{\mathbf{G}}} e^{i\tilde{\mathbf{G}}(\mathbf{r}-\mathbf{r}')} \varepsilon(\tilde{\mathbf{k}} + \tilde{\mathbf{G}}) \\ &= \frac{L_c}{L} \sum_{\tilde{\mathbf{R}}\tilde{\mathbf{R}}'} e^{-i\tilde{\mathbf{k}}(\tilde{\mathbf{R}}+\mathbf{r}-\tilde{\mathbf{R}}'-\mathbf{r}')} t_{\tilde{\mathbf{R}}+\mathbf{r}, \tilde{\mathbf{R}}'+\mathbf{r}'} \\ &= e^{-i\tilde{\mathbf{k}}(\mathbf{r}-\mathbf{r}')} t_{rr'}(\tilde{\mathbf{k}}). \end{aligned} \quad (59)$$

This is very easily implemented numerically. The DCA self-consistency condition reads

$$G_{rr'}^{(\text{cluster})}(\omega) = G_{rr'}^{(\text{loc})}(\omega) = \frac{L_c}{L} \sum_{\tilde{\mathbf{k}} \in \mathcal{RSC}} \left(\frac{1}{\omega + \mu - \bar{\mathbf{t}}(\tilde{\mathbf{k}}) - \Sigma(\omega)} \right)_{rr'}. \quad (60)$$

The decisive difference as compared to the C-DMFT is that $\bar{\mathbf{t}}$ is also invariant under cyclic cluster translations, as it is the case for \mathbf{t}' . Hence, all matrices are simultaneously diagonalized by the cluster Fourier transformation \mathbf{W} , and we get a scalar self-consistency equation

$$G^{(\text{cluster})}(\tilde{\mathbf{G}}, \omega) = \frac{L_c}{L} \sum_{\tilde{\mathbf{k}}} \frac{1}{\omega + \mu - \varepsilon(\tilde{\mathbf{k}} + \tilde{\mathbf{G}}) - \Sigma(\tilde{\mathbf{G}}, \omega)}. \quad (61)$$

Which of the three cluster approaches, the C-DMFT, the PC-DMFT, and the DCA is the best one? This is a question that comes up immediately. An answer could be expected from a meta theory unifying all cluster approaches in a common theoretical framework. The self-energy-functional theory (SFT) [34, 10, 6] is in fact able to re-derive various approximations as stationary points of a general functional $\Omega_{\mathbf{t}, \mathbf{U}}[\Sigma]$ for a given original lattice model with parameters \mathbf{t} and \mathbf{U} . A particular approximation is defined by the choice of a reference system, with possibly different one-particle parameters \mathbf{t}' but the same interaction \mathbf{U} . The reference system could be a system of decoupled clusters, also including noninteracting bath degrees of freedom, and is fixed by the structure of the \mathbf{t}' matrix. The self-energy of the reference system, $\Sigma_{\mathbf{t}', \mathbf{U}}(\omega)$ is considered as a trial self-energy which must be optimized via the stationarity condition

$$\partial\Omega_{t,U}[\Sigma_{t',U}]/\partial t' = 0 , \quad (62)$$

i.e., the self-energy is optimized by varying the one-particle parameters of the reference system. Taking the single-impurity Anderson model, Eq. (51), as a reference system, Eq. (62) recovers the DMFT self-consistency condition. For an Anderson cluster model, Eq. (55), the C-DMFT self-consistency condition is found. The DCA is obtained with the same reference system (with periodic boundaries) but applied to a different original model with t replaced by \bar{t} . Thereby, a set of external parameters of the self-energy functional is changed, $\Omega_{t,U}[\Sigma] \rightarrow \Omega_{\bar{t},U}[\Sigma]$, such that an unbiased comparison of the resulting optimal free energies is not possible. In case of the PC-DMFT, the parameters t and U remain unchanged, and the PC-DMFT self-consistency equation is also re-derived with the same reference system. Unfortunately, the form of the self-energy functional must be changed for this purpose, $\Omega_{t,U}[\Sigma] \rightarrow \Omega_{t,U}[\hat{T}[\Sigma]]$, and this means that a fair comparison is again not possible. One should note that the modification of the parameters of the original system (DCA) or the modification of the functional form (PC-DMFT) keep the systematic nature of the approach, i.e., they become irrelevant in the infinite-cluster limit and must therefore be considered as formally well justified. The SFT does provide the expected hierarchy among different approaches within each row of Tab. 2. E.g. the C-DMFT must be seen as superior compared to the CPT. In between, we find the variational cluster approach (VCA) which is defined by the same reference system as used for the CPT but with variational optimization of the intra-cluster hopping and the one-particle energies. There is also an interesting new approximation suggesting itself: Starting with the modified hopping \bar{t} and the reference system in Fig. 9b, generates a simplified DCA without bath degrees of freedom. This stands between the periodic CPT and the full DCA, see last row of Tab. 2.

Another criterion to decide between the different cluster approaches, could be their convergence behavior for $L_c \rightarrow \infty$. Consider first a *local* observable, such as the double occupancy in the Hubbard model or the local density of states, at a central site in an isolated cluster with L_c sites. Since nonlocal elements of Green functions typically decay exponentially with increasing distance, if the system is not at a critical point, one would expect an exponentially fast convergence of the observable with $L_c \rightarrow \infty$. This is the case for the C-DMFT, as the bath only couples to the surface sites of the cluster (assuming hopping between nearest neighbors only). The latter is easily seen by expanding both sides of the C-DMFT self-consistency equation, $G_{rr'}^{(\text{cluster})}(\omega) = G_{rr'}^{(\text{loc})}(\omega)$, and Eq. (57) in powers of $1/\omega$ keeping terms of the order $1/\omega^3$, which eventually implies $V_{rk} \neq 0$ for surface sites r only. Extended observables, e.g., the \mathbf{k} -dependent Green function or the free energy, converge to the exact results with corrections $\sim 1/L_1$, where $L_c = L_1^D$ for a D -dimensional hypercubic cluster. This is obvious since only $2DL_1^{D-1}$ surface sites contribute to the average hybridization function compared to the total number of cluster sites L_1^D . For the DCA, on the other hand, where all sites in the cluster are coupled to the bath, convergence is faster with corrections $\sim 1/L_c^2$. A detailed discussion can be found in Ref. [5]. One should keep in mind, however, that with the cluster sizes that can be treated in practical calculations one is typically far from the regime where this scaling behavior can be seen.

A further important issue to be discussed is the description of *spontaneous* breaking of translational symmetry, e.g., in antiferromagnetic phases, charge-density-wave states, stripe order etc. Within the C-DMFT, if the cluster is large enough to contain the new unit cell, such phases can be found easily as there is no assumption made on the translational symmetry of the cluster self-energy. The DCA, on the other hand, does require translation symmetry on the cluster when using the self-consistency equation (61) formulated in reciprocal space. Symmetry breaking must then be anticipated and, considering e.g. antiferromagnetic order, one must introduce a reduced Brillouin zone and a constraint for the self-energy relating \mathbf{k} and $\mathbf{k} + \mathbf{Q}_{\text{AF}}$, where \mathbf{Q}_{AF} determines the type of antiferromagnetic ordering. The real-space formulation, Eq. (60) is much more elegant, as translation symmetry in the cluster can be broken spontaneously and arbitrarily, such that there is no need to anticipate a specific ordering pattern. In any case and for both, C-DMFT and DCA, it is clear, however, that a selected cluster size and cluster shape will necessarily bias to some degree the spatial modulation of the order parameter one is looking for. Calculations with different cluster geometries and sizes are therefore necessary. This must be seen as a big intrinsic disadvantage of the cluster approach. Finally, the description of the broken translation symmetries in the PC-DMFT is much more complicated and is discussed in Ref. [31], for example.

9 Discussion of selected results

One of the main topics of DMFT is the Mott metal-insulator transition in the Hubbard model [4]. For $U = 0$ the system is a noninteracting metallic Fermi gas while for strong U the zero-temperature phase is a Mott insulator due to the high penalty for hopping processes producing doubly occupied sites. As a function of U , the single-site DMFT predicts a continuous metal-insulator transition at $T = 0$, see the $T = 0$ end of the dashed line in Fig. 11 (left) [35]. The yellow area marks a coexistence regime, where the metallic and the insulating solution of the DMFT coexist. At finite temperatures, the free energy decides which one is stable, and the transition becomes discontinuous with a jump of, e.g., the double occupancy at the critical interaction $U_c(T)$. The dashed line of first order transitions ends in a second-order critical end point at U_{MIT} . At still higher temperatures there is a smooth crossover only, separating a bad-metal from a bad-insulator regime. The phase diagram, calculated for the Hubbard model on the square lattice, has the same structure as the corresponding phase diagram for the $D = \infty$ hypercubic lattice. This unphysical essential independence of the results on the lattice dimension is characteristic for a mean-field approach. There is another serious problem. Namely, there is a macroscopically high entropy of the $T = 0$ Mott-insulating ground state due to the 2^L -fold degeneracy with respect to the orientation of the local magnetic moments. Within the DMFT, this degeneracy can only be lifted by long-range magnetic order, and in fact in the true DMFT ground state the system is an antiferromagnetic insulator for strong U . As has been discussed above (see Fig. 5), this is due to the superexchange mechanism favoring antiferromagnetic alignment of neighboring moments. This Heisenberg-insulator state, however, is suppressed in the DMFT calculation by enforcing spin symmetric solutions. The motivation is

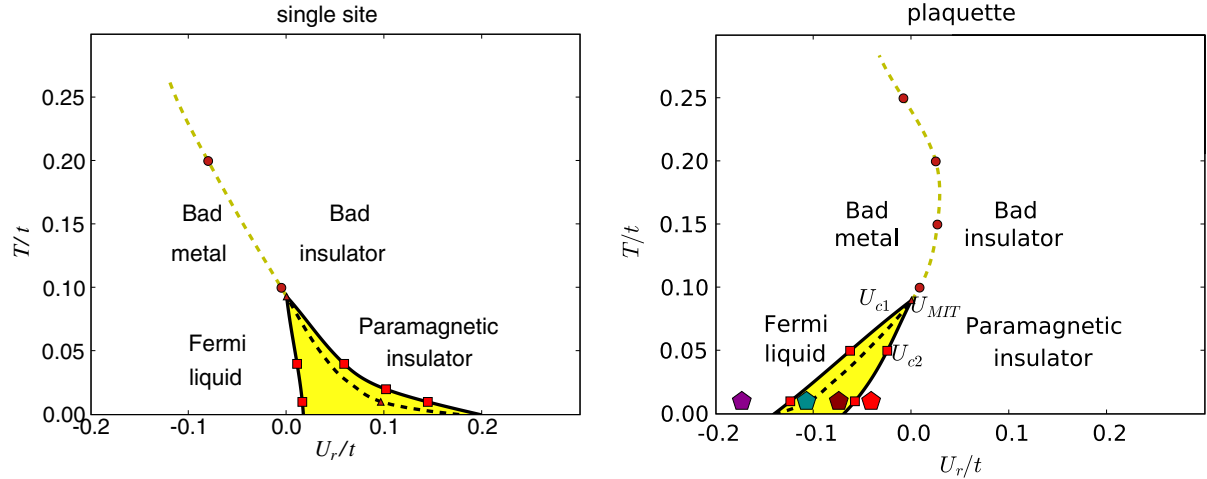


Fig. 11: Phase diagram of the paramagnetic Hubbard model at half-filling on the square lattice. Left: single-site DMFT. Right: C-DMFT, $L_c = 4$. $U_r \equiv (U - U_{\text{MIT}})/U_{\text{MIT}}$ with $U_{\text{MIT}} = 9.35t$ (DMFT), $U_{\text{MIT}} = 6.05t$ (C-DMFT). Reprinted figure with permission from [35]. Copyright (2008) by the American Physical Society.

to uncover in this way the Mott transition in the paramagnetic state at temperatures below the Néel temperature $T_N(U)$. In the paramagnetic state and at finite temperatures, the large entropy stabilizes the Mott insulator as compared to the metallic Fermi-liquid state.

The C-DMFT can cure this defect since it incorporates the feedback of short-range antiferromagnetic correlations, i.e., the spin degeneracy can be lifted by forming a nonlocal spin-singlet state on neighboring sites *within* the reference system and thus corrects the cluster self-energy. Fig. 11 (right) shows the phase diagram as obtained with a $L_c = 4$ -site (plaquette) calculation. It turns out that salient features of the DMFT phase diagram are preserved. In particular, there is again a coexistence of a metallic and an insulating phase in a certain U - T range of the phase diagram, and a first-order transition line separating the metallic Fermi liquid at weaker U from the Mott insulator at stronger U . On the other hand, there are a couple of differences: First of all, the critical interaction is substantially reduced (see caption of Fig. 11). Second, the line of first-order transitions remains first order down to $T = 0$, i.e., the $T = 0$ Mott transition is discontinuous rather than continuous as predicted by DMFT, see Ref. [36]. Most important, however, as the insulating phase at low temperatures now has a very small entropy, a decreasing temperature favors the insulator over the metal. At high temperatures, one expects and finds the same trend of the crossover lines since here correlations are broken up thermally. At low T , however, the first-order transition line bends back, and $U_c(T)$ decreases with decreasing T .

The importance of short-range antiferromagnetic correlations is also highlighted by the local spectral function $A(\omega)$ calculated within the DCA for $L_c = 4$ shown in Fig. 12 [37]. Note that $A(\omega)$ (black solid line) is slightly asymmetric. This is a slight artifact of the maximum-entropy method that must be employed to obtain real-frequency data from the Green function given on the Matsubara frequencies on the imaginary- ω axis, on which the numerical evaluation of the theory must be implemented when using a quantum Monte-Carlo cluster solver. Still there is a clear four-peak structure visible in $A(\omega)$. This exactly in line with the lattice QMC results shown in Fig. 3. Hence, one would expect that the low-excitation-energy peaks signal

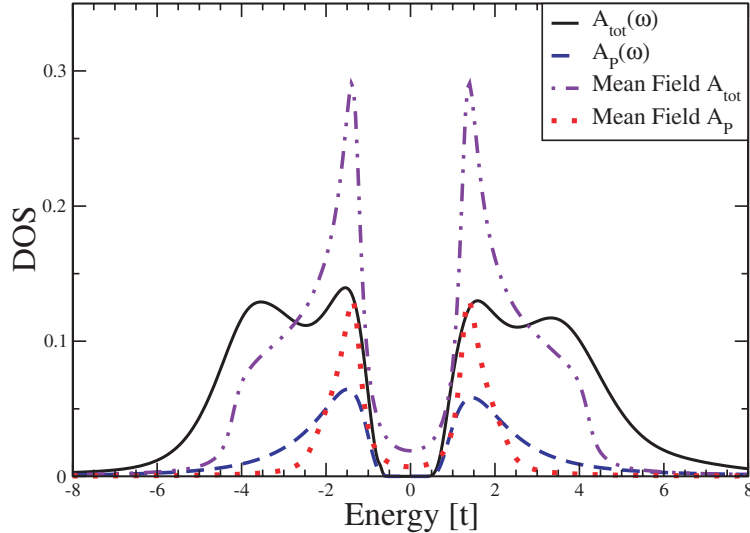


Fig. 12: Local density of states $A(\omega)$ for the half-filled Hubbard model at $U = 6t$ as obtained by the DCA with $L_c = 4$. Figure adapted from Ref. [37].

nonlocal antiferromagnetic correlations. This is corroborated by comparing with the spectral density obtained by a static (Hartree-Fock) mean-field calculation for the symmetry-broken antiferromagnetic state with the same gap (see dash-dotted line). The similarity to the DCA results in the low-frequency range emphasizes the importance of nonlocal correlations again. More than this, it also suggests that the gap is not necessarily a Mott-Hubbard gap but rather a “Slater” gap. In the static mean-field Slater theory, long-range antiferromagnetic order implies a doubling of the unit cell with a gap opening at the boundary of the reduced Brillouin zone.

The Mermin-Wagner theorem [17] actually excludes a spontaneous breaking of the SU(2) spin-rotational symmetry at any finite temperature in two spatial dimensions. Hence, antiferromagnetic order obtained in the static mean-field theory but also in the C-DMFT and DCA at low but finite temperatures (if solutions are not enforced to be spin-symmetric) must be seen as artifacts. However, this does not imply that the Slater mechanism for the gap opening is irrelevant. Namely, for small clusters, the antiferromagnetic correlation length well exceeds the linear cluster extension at low T . It has, indeed, been suggested that the metal-insulator transition is in fact of the Slater type in $D = 2$ [37]. However, another important observation is that the transition is orbital (or \mathbf{k}) selective [35, 36]. In the $L_c = 4$ calculation, two of the orbitals $(\pi, 0)$ and $(0, \pi)$ exhibit a Mott-like transition where the spectral gap is opened because the self-energy $\Sigma_{(\pi,0)}(\omega)$ develops a pole at $\omega = 0$ while the remaining orbitals $(0, 0)$ and (π, π) undergo a Slater-type transition. In a single-site mean-field theory, on the other hand, such momentum-space differentiation is impossible.

More recent studies [38] using lattice QMC as well as the DΓA, a diagrammatic extension of DMFT [39], demonstrate that at low temperatures strong nonlocal antiferromagnetic correlations are responsible for opening a gap even at arbitrarily weak U . The system evolves from a Slater-like to a Heisenberg-like antiferromagnet at low but finite T but without explicitly breaking the SU(2) symmetry. This implies that actually no metal-insulator transition can be identified for $D = 2$ and that the system is a paramagnetic insulator for all U .

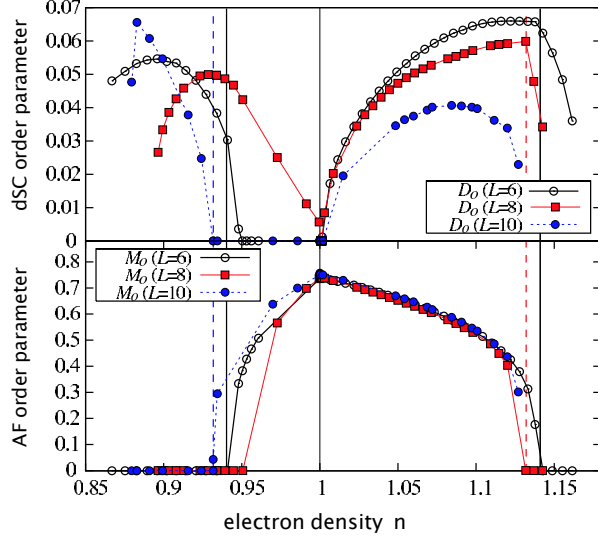


Fig. 13: Superconducting (top) and antiferromagnetic order parameter (bottom) as a function of the electron density n in the $D = 2$ Hubbard model at $T = 0$ and $U = 8t$. VCA results for different clusters: 2×3 -, 2×4 - and 10 -site clusters. Reprinted figure with permission from [40]. Copyright (2005) by the American Physical Society.

Let us finally discuss an application of a cluster approach to the $D = 2$ Hubbard model which focusses on unconventional d -wave superconductivity. At zero temperature, spontaneous symmetry breaking is no longer excluded by the Mermin-Wagner theorem. A single-site mean-field theory, however, cannot treat symmetry-broken phases that are characterized by *nonlocal* order parameters. Fig. 13 displays results obtained by means of the VCA [40] for the Hubbard model on the $D = 2$ square lattice with nearest-neighbor ($t = 1$), next-nearest-neighbor diagonal ($t' = -0.3$) and third-neighbor hopping ($t'' = 0.2t$) at $U = 8t$ and $T = 0$. Within the VCA, there is no bath continuum to be optimized but two symmetry-breaking Weiss fields which couple to the reference system H' of disconnected clusters. In particular,

$$H'_M = \sum_i (-1)^i (n_{i\uparrow} - n_{i\downarrow}) \quad (63)$$

probes antiferromagnetic order and

$$H'_D = \sum_{ij} \Delta_{ij} (c_{i\uparrow} c_{j\downarrow} + \text{H.c.}) \quad (64)$$

d -wave superconductivity with $\Delta_{ij} = D$ if sites i, j are nearest neighbors along the x axis and $\Delta_{ij} = -D$ if sites i, j are nearest neighbors along the y axis. The corresponding AF and SC order parameters, M_{AF} and D_{SC} can be obtained from the normal and from the anomalous elements of the one-particle Green function in the Nambu formalism (see Ref. [40] for details) and are plotted in Fig. 13 as function of the filling n . The figure demonstrates that antiferromagnetism persists up to about $\delta \equiv |1 - n| = 15\%$ doping on the electron-doped side ($n > 1$) and about 6% on the hole-doped side. Superconductivity coexists with antiferromagnetism, but a pure SC phase is found as well, particularly at higher hole-doping levels. Unfortunately, there are strong finite-size and cluster-geometry effects such that, even if these results are physically very appealing and plausible, improved and more systematic cluster calculations are necessary to prove that the $D = 2$ Hubbard model has a d -wave superconducting ground state.

10 Conclusions and open problems

Dynamical mean-field theory is in many cases too strong an approximation for the description of physical phenomena in low-dimensional lattice models. Conceptually, cluster extensions of the DMFT are highly important as they are able to bridge the gap between the single-site mean-field approach and the exact solution. In practice, however, it very much depends on the capabilities of the “cluster solver” if the cluster size L_c that can still be treated numerically is sufficiently large. In almost all interesting cases, i.e., for not too high temperatures etc., the accessible cluster sizes are unfortunately too small to allow for a systematic and reliable finite-size scaling, and thus we have to await further progress in the development of solver techniques (see Ref. [41], for example).

Still the cluster concept represents a big step forward. Its predictions can be checked systematically by comparing results for different cluster sizes, it provides complementary information to plain finite-size simulations, and it does account for important physics that is not captured by the single-site DMFT. In particular, by self-consistent mapping of the lattice problem onto a cluster with $L_c > 1$, it is possible to include the feedback of nonlocal two-particle correlations on the one-particle quantities, such as the formation of nonlocal opposed to local spin singlets. Nonlocal correlations on the length scale given by the linear extension of the cluster are treated accurately, while longer-range correlations are captured on the static mean-field level only.

The application of a cluster approach is thus advisable whenever the physics is crucially affected by nonlocal but short-range correlations. This is the case for the Mott transition in two dimensions, for example [35,36,38]. To describe phases with spontaneously broken symmetries that are characterized by a nonlocal order parameter, such as unconventional d -wave superconductivity, a cluster approach is even necessary.

The cluster extension of the DMFT is not unique. Among the various different approaches, the cellular DMFT and the dynamical cluster approximation are the most popular. Both are clearly superior as compared to the more simple cluster-perturbation theory. The variational cluster approximation stands in between and is attractive if an exact-diagonalization-based cluster solver shall be employed. If an absent or mild the fermionic sign problem permits the use of a quantum Monte-Carlo solver, the C-DMFT or DCA represent the methods of choice since the treatment of the noninteracting bath degrees of freedom comes “for free” and even tend to attenuate the sign problem. The periodized cellular approach is closely related but appears a bit inconvenient when systems with broken translation symmetries shall be studied. As a rule of thumb, the C-DMFT is preferable if local quantities are addressed while observables extending over the cluster size converge faster with increasing L_c within the DCA.

One should also be aware about a couple of remaining problems. Common to all cluster techniques is the problem that translation symmetries are broken artificially, as is most obvious in the CPT and the C-DMFT. Additional periodization schemes must be employed which, however, have some *ad hoc* character and do not remove a possible intrinsic bias of the approximation when studying phase diagrams involving spontaneously broken translation symmetries. The DCA involves a periodization scheme at a deeper level but is also not free of related artifacts

such as the discontinuous k -dependence of the self-energy. A problem related to artificially broken translation symmetries is given by lattice models with strongly reduced or even absent translation symmetries, such as impurities in a correlated lattice, nanostructures at solid surfaces, etc. Opposed to the real-space DMFT for inhomogeneous systems, there is no straightforward inhomogeneous cluster approach. Another problem, already present on the single-site mean-field level, is the proper treatment of models with nonlocal or even long-ranged interactions. Here, the cluster concept would allow for an explicit consideration of short-range nonlocal interactions on the scale of the cluster while an additional static mean-field decoupling was required for interaction terms across the cluster boundaries. There are, however, other and probably superior ways to tackle this problem, such as extended DMFT [42] or the dual-boson method [43].

Diagrammatic routes to treat nonlocal correlations beyond dynamical mean-field theory [39] represent a very promising alternative to cluster approaches. Here, the idea is compute corrections to the DMFT self-energy through additional Feynman diagrams and to start from a local approximation for the two-particle vertex instead of the bare Coulomb interaction as a building block. One of the big advantages is that nonlocal correlations can be accounted for without breaking translational symmetries. Compared to cluster extensions of DMFT, however, diagrammatic routes appear less systematic in approaching the full solution of correlated lattice fermion models.

References

- [1] W. Metzner and D. Vollhardt, Phys. Rev. Lett. **62**, 324 (1989)
- [2] A. Georges and G. Kotliar, Phys. Rev. B **45**, 6479 (1992)
- [3] M. Jarrell, Phys. Rev. Lett. **69**, 168 (1992)
- [4] A. Georges, G. Kotliar, W. Krauth, and M.J. Rozenberg, Rev. Mod. Phys. **68**, 13 (1996)
- [5] T. Maier, M. Jarrell, T. Pruschke, and M.H. Hettler, Rev. Mod. Phys. **77**, 1027 (2005)
- [6] M. Potthoff, in A. Avella and F. Mancini (eds.): *Strongly Correlated Systems: Theoretical Methods*, Springer Series in Solid-State Sciences, Vol. 171, p. 303 (Springer, Berlin, 2012)
- [7] M.H. Hettler, A.N. Tahvildar-Zadeh, M. Jarrell, T. Pruschke, and H.R. Krishnamurthy, Phys. Rev. B **58**, R7475 (1998)
- [8] A.I. Lichtenstein and M.I. Katsnelson, Phys. Rev. B **62**, R9283 (2000)
- [9] G. Kotliar, S.Y. Savrasov, G. Pálsson, and G. Biroli, Phys. Rev. Lett. **87**, 186401 (2001)
- [10] M. Potthoff, M. Aichhorn, and C. Dahnken, Phys. Rev. Lett. **91**, 206402 (2003)
- [11] A.C. Hewson: *The Kondo Problem to Heavy Fermions* (Cambridge Univ. Press, 1993)
- [12] T. Moriya: *Spin Fluctuations in Itinerant Electron Magnetism*, Springer Series in Solid-State Sciences, Vol. 56 (Springer, Berlin, 1985)
- [13] H. Capellmann (Ed.): *Metallic Magnetism*, Springer Topics in Current Physics, Vol. 42 (Springer, Berlin, 1987)
- [14] N.M. Plakida: *High-Temperature Superconductivity* (Springer, Berlin, 1993)
- [15] J.R. Waldram: *Superconductivity of Metals and Cuprates* (IOP Publishing, London, 1996)
- [16] F. Gebhard: *The Mott Metal-Insulator Transition* (Springer, Berlin, 1997)
- [17] N.D. Mermin and H. Wagner, Phys. Rev. Lett. **17**, 1133 (1966)
- [18] J. Hubbard, Proc. R. Soc. London A **276**, 238 (1963)
- [19] M.C. Gutzwiller, Phys. Rev. Lett. **10**, 159 (1963)
- [20] J. Kanamori, Prog. Theor. Phys. (Kyoto) **30**, 275 (1963)
- [21] C. Gröber, R. Eder, and W. Hanke, Phys. Rev. B **62**, 4336 (2000)
- [22] C. Dahnken, M. Aichhorn, W. Hanke, E. Arrigoni, and M. Potthoff, Phys. Rev. B **70**, 245110 (2004)

- [23] F.H.L. Essler, H. Frahm, F. Göhmann, A. Klümper, and V. Korepin: *The One-Dimensional Hubbard Model* (Cambridge University Press, 2005)
- [24] C. Gros and R. Valenti, Phys. Rev. B **48**, 418 (1993)
- [25] D. Sénéchal, D. Pérez, and M. Pioro-Ladrière, Phys. Rev. Lett. **84**, 522 (2000)
- [26] M. Potthoff: *Making use of self-energy functionals: The variational cluster approximation*, in E. Pavarini, E. Koch, D. Vollhardt, and A. Lichtenstein (eds.): *DMFT at 25: Infinite Dimensions, Modeling and Simulation*, Vol. 4 (FZ Jülich, 2014)
- [27] D. Sénéchal, in A. Avella and F. Mancini (eds.): *Strongly Correlated Systems: Theoretical Methods*, Springer Series in Solid-State Sciences, Vol. 171, p. 237 (Springer, Berlin, 2012)
- [28] M.G. Zacher, R. Eder, E. Arrigoni, and W. Hanke, Phys. Rev. Lett. **85**, 2585 (2000)
- [29] D. Sénéchal, D. Pérez, and D. Plouffe, Phys. Rev. B **66**, 075129 (2002)
- [30] T. Minh-Tien, Phys. Rev. B **74**, 155121 (2006)
- [31] G. Biroli, O. Parcollet, and G. Kotliar, Phys. Rev. B **69**, 205108 (2004)
- [32] E. Müller-Hartmann, Z. Phys. B **76**, 211 (1989)
- [33] M. Potthoff and W. Nolting, Phys. Rev. B **59**, 2549 (1999)
- [34] M. Potthoff, Euro. Phys. J. B **32**, 429 (2003)
- [35] H. Park, K. Haule, and G. Kotliar, Phys. Rev. Lett. **101**, 186403 (2008)
- [36] M. Balzer, B. Kyung, D. Sénéchal, A.-M.S. Tremblay, and M. Potthoff, Europhys. Lett. **85**, 17002 (2009)
- [37] E. Gull, P. Werner, X. Wang, M. Troyer, and A.J. Millis, Europhys. Lett. **84**, 37009 (2008)
- [38] T. Schäfer, F. Geles, D. Rost, G. Rohringer, E. Arrigoni, K. Held, N. Blümer, M. Aichhorn, and A. Toschi, Phys. Rev. B **91**, 125109 (2015)
- [39] G. Rohringer, H. Hafermann, A. Toschi, A.A. Katanin, A.E. Antipov, M.I. Katsnelson, A.I. Lichtenstein, A.N. Rubtsov, and K. Held, Rev. Mod. Phys. **90**, 025003 (2018)
- [40] D. Sénéchal, P.-L. Lavertu, M.-A. Marois, and A.-M.S. Tremblay, Phys. Rev. Lett. **94**, 156404 (2005)
- [41] E. Gull, A. Millis, A. Lichtenstein, A. Rubtsov, M. Troyer, and P. Werner, Rev. Mod. Phys. **83**, 349 (2011)
- [42] R. Chitra and G. Kotliar, Phys. Rev. Lett. **84**, 3678 (2000)
- [43] A.N. Rubtsov, M.I. Katsnelson, and A.I. Lichtenstein, Ann. Phys. (N.Y.) **327**, 1320 (2012)